

# 1 Methane mapping, emission quantification, and attribution in two 2 European cities; Utrecht, NL and Hamburg, DE

3 Hossein Maazallahi<sup>1,2</sup>, Julianne M. Fernandez<sup>3</sup>, Malika Menoud<sup>1</sup>, Daniel Zavala-Araiza<sup>1,4</sup>,  
4 Zachary D. Weller<sup>5</sup>, Stefan Schwietzke<sup>6</sup>, Joseph C. von Fischer<sup>7</sup>, Hugo Denier van der Gon<sup>2</sup>, and  
5 Thomas Röckmann<sup>1</sup>

6 <sup>1</sup>Institute for Marine and Atmospheric research Utrecht (IMAU), Utrecht University (UU), Utrecht, The Netherlands

7 <sup>2</sup>Netherlands Organisation for Applied Scientific Research (TNO), Utrecht, The Netherlands

8 <sup>3</sup>Department of Earth Sciences, Royal Holloway University of London (RHUL), Egham, United Kingdom

9 <sup>4</sup>Environmental Defense Fund (EDF), Utrecht, The Netherlands

10 <sup>5</sup>Department of Statistics, Colorado State University (CSU), United States of America

11 <sup>6</sup>Environmental Defense Fund (EDF), Berlin, Germany

12 <sup>7</sup>Department of Biology, Colorado State University (CSU), United States of America

13 *Correspondence to:* Hossein Maazallahi (h.maazallahi@uu.nl)

14 **Abstract.** Characterizing and attributing methane (CH<sub>4</sub>) emissions across varying scales is important from environmental,  
15 safety, and economic perspectives, and is essential for designing and evaluating effective mitigation strategies. Mobile real-  
16 time measurements of CH<sub>4</sub> in ambient air offer a fast and effective method to identify and quantify local CH<sub>4</sub> emissions in  
17 urban areas. We carried out extensive campaigns to measure CH<sub>4</sub> mole fractions at the street level in Utrecht, The Netherlands  
18 (2018 and 2019) and Hamburg, Germany (2018). We detected 145 leak indications (LIs, i.e., CH<sub>4</sub> enhancements of more than  
19 10% above background levels) in Hamburg and 81 LIs in Utrecht. Measurements of the ethane-to-methane ratio (C<sub>2</sub>:C<sub>1</sub>),  
20 methane-to-carbon dioxide ratio (CH<sub>4</sub>:CO<sub>2</sub>), and CH<sub>4</sub> isotope composition ( $\delta^{13}\text{C}$  and  $\delta\text{D}$ ) show that in Hamburg about 1/3 of  
21 the LIs, and in Utrecht 2/3 of the LIs (based on a limited set of C<sub>2</sub>:C<sub>1</sub> measurements), were of fossil fuel origin. We find that  
22 in both cities the largest emission rates in the identified LI distribution are from fossil fuel sources. In Hamburg,  
23 the lower emission rates in the identified LI distribution are often associated with biogenic characteristics, or partly  
24 combustion. Extrapolation of detected LI rates along the roads driven to the gas distribution pipes in the entire road network  
25 yields total emissions from sources that can be quantified in the street-level surveys of  $440 \pm 70 \text{ t yr}^{-1}$  from all sources in  
26 Hamburg, and  $150 \pm 50 \text{ t yr}^{-1}$  for Utrecht. In Hamburg, C<sub>2</sub>:C<sub>1</sub>, CH<sub>4</sub>:CO<sub>2</sub>, and isotope-based source attributions shows that 50  
27 - 80 % of all emissions originate from the natural gas distribution network, in Utrecht more limited attribution indicates that  
28 70 - 90 % of the emissions are of fossil origin. Our results confirm previous observations that a few large LIs, creating a heavy  
29 tail, are responsible for a significant proportion of fossil CH<sub>4</sub> emissions. In Utrecht, 1/3 of total emissions originated from one  
30 LI and in Hamburg >1/4 from 2 LIs. The largest leaks were located and fixed quickly by GasNetz Hamburg once the LIs were  
31 shared, but 80 % of the (smaller) LIs attributed to the fossil category could not be detected/confirmed as pipeline leaks. This  
32 issue requires further investigation.

## 33 1 Introduction

34 Methane (CH<sub>4</sub>) is the second most important anthropogenic greenhouse gas (GHG) after carbon dioxide (CO<sub>2</sub>) with  
35 a global warming potential of 84 compared to CO<sub>2</sub> over a 20-year time horizon (Myhre et al., 2013). The increase of CH<sub>4</sub> mole  
36 fraction from about 0.7 parts per million (ppm) or 700 parts per billion (ppb) in pre-industrial times (Etheridge et al., 1998;  
37 MacFarling Meure et al., 2006) to almost 1.8 ppm at present (Turner et al., 2019) is responsible for about 0.5 W m<sup>-2</sup> of the  
38 total 2.4 W m<sup>-2</sup> radiative forcing since 1750 (Etminan et al., 2016; Myhre et al., 2013). In addition to its direct radiative effect,  
39 CH<sub>4</sub> plays an important role in tropospheric chemistry and affects the mixing ratio of other atmospheric compounds, including  
40 direct and indirect greenhouse gases, via reaction with the hydroxyl radical (OH), the main loss process of CH<sub>4</sub> (Schmidt and

41 Shindell, 2003). In the stratosphere CH<sub>4</sub> is the main source of water vapor (H<sub>2</sub>O) (Noël et al., 2018), which adds another aspect  
42 to its radiative forcing. Via these interactions the radiative impact of CH<sub>4</sub> is actually higher than what can be ascribed to its  
43 mixing ratio increase alone, and the total radiative forcing ascribed to emissions of CH<sub>4</sub> is estimated to be almost 1 W m<sup>-2</sup>, ≈  
44 60 % of that of CO<sub>2</sub> (Fig 8.17 in Myhre et al., 2013). Given this strong radiative effect, and its relatively short atmospheric  
45 lifetime of about 9.1 ± 0.9 yr (Prather et al., 2012), CH<sub>4</sub> is an attractive target for short- and medium-term mitigation of global  
46 climate change as mitigation will yield rapid reduction in warming rates.

47 CH<sub>4</sub> emissions originate from a wide variety of natural and anthropogenic sources, for example emissions from  
48 natural wetlands, agriculture (e.g. ruminants or rice agriculture), waste decomposition, or emissions (intended and non-  
49 intended) from oil and gas activities that are associated with production, transport, processing, distribution, and end-use of  
50 fossil fuel sector (Heilig, 1994). Fugitive unintended and operation-related emissions occur across the entire oil and natural  
51 gas supply chain. In the past decade, numerous large studies have provided better estimates of the emissions from extended  
52 oil and gas production basins (Allen et al., 2013; Karion et al., 2013; Omara et al., 2016; Zavala-Araiza et al., 2015; Lyon et  
53 al., 2015), the gathering and processing phase (Mitchell et al., 2015), and transmission and storage (Zimmerle et al., 2015;  
54 Lyon et al., 2016) in the United States (US). A recent synthesis concludes that the national emission inventory of the US  
55 Environmental Protection Agency (EPA) underestimated supply chain emissions by as much as 60 % (Alvarez et al., 2018).  
56 McKain et al. (2015) discussed how inventories may underestimate the total CH<sub>4</sub> emission for cities. Also, an analysis of  
57 global isotopic composition data suggests that fossil related emissions may be 60 % higher than what has been previously  
58 estimated (Schwietzke et al., 2016). A strong underestimate of fossil fuel related emissions of CH<sub>4</sub> was also implied by analysis  
59 of δ<sup>14</sup>C-CH<sub>4</sub> in pre-industrial air (Hmiel et al., 2020). These emissions do not only have adverse effects on climate, but also  
60 represent an economic loss (Xu and Jiang, 2017) and a potential safety hazard (West et al., 2006). While CH<sub>4</sub> is the main  
61 component in natural gas distribution networks (NGDNs), composition of natural gas varies from one country or region to  
62 another. In Europe the national authorities provide specifications on components of natural gas in the distribution network  
63 (Table 8 in UNI MISKOLC and ETE, 2008).

64 Regarding CH<sub>4</sub> emissions from NGDNs, a number of intensive CH<sub>4</sub> surveys with novel mobile high precision laser-  
65 based gas analyzers in US cities have recently revealed the widespread presence of leak indications (LIs: CH<sub>4</sub> enhancements  
66 of more than 10 % above background level) with a wide range of magnitudes (Weller et al., 2020; Weller et al., 2018; von  
67 Fischer et al., 2017; Chamberlain et al., 2016; Hopkins et al., 2016; Jackson et al., 2014; Phillips et al., 2013). The number and  
68 severity of natural gas leaks appears to depend on pipeline material and age, local environmental conditions, pipeline  
69 maintenance and replacement programs (von Fischer et al., 2017; Gallagher et al., 2015; Hendrick et al., 2016). For example,  
70 NGDNs in older cities with a larger fraction of cast iron or bare steel pipes showed more frequent leaks than NGDNs that use  
71 the newer plastic pipes. The data on CH<sub>4</sub> leak indications from distribution systems in cities have provided valuable data for  
72 emission reduction in the US cities which allows local distribution companies (LDCs) who are in charge of NGDN to quickly  
73 fix leaks and allocate resources efficiently (Weller et al., 2018, von Fischer et al., 2017, Lamb et al., 2016; McKain et al.,  
74 2015).

75 Urban European cities CH<sub>4</sub> emissions are not well known, which requires carrying out extensive campaigns to collect  
76 required observation data. Few studies have estimated urban CH<sub>4</sub> fluxes using eddy covariance measurements (Gioli et al.,  
77 2012; Helfter et al., 2016), airborne mass balance approaches (O'Shea et al., 2014) and the Radon-222 flux and mixing layer  
78 height techniques (Zimnoch et al., 2019). Gioli et al. (2012) showed that about 85 % of methane emissions in Florence, Italy  
79 originated from natural gas leaks. Helfter et al. (2016) estimated CH<sub>4</sub> emissions of 72 ± 3 t km<sup>-2</sup> yr<sup>-1</sup> in London, UK mainly  
80 from sewer sesystem and NGDNs leaks, which is twice as much as reported in the London Atmospheric Emissions Inventory.  
81 O'Shea et al. (2014) also showed that CH<sub>4</sub> emissions in greater London is about 3.4 times larger than the report from UK  
82 National Atmospheric Emission Inventory. Zimnoch et al. (2019) estimated CH<sub>4</sub> emissions of (6.2 ± 0.4) × 10<sup>6</sup> m<sup>3</sup> year<sup>-1</sup> for

83 Krawko, Poland, based on data for the period of 2005 to 2008 and concluded that leaks from NGDNs are the main emission  
84 source in Krawko, based on carbon isotopic signature of CH<sub>4</sub>. Chen et al. (2020) also showed that incomplete combustion or  
85 loss from temporarily installed natural gas appliances during big festivals can be the major source of CH<sub>4</sub> emissions from such  
86 events, while these emissions have not been included in inventory reports for urban emissions.

87 Here we present the result of mobile in-situ measurements at street level for whole-city surveys in two European  
88 cities, Utrecht in the Netherlands (NL) and Hamburg in Germany (DE). In this study, we quantified LIs emissions using an  
89 empirical equation from Weller et al. (2019), which was designed based on controlled release experiments from von Fischer  
90 et al. (2017), to quantify ground-level emissions locations in urban area such as leaks from NGDN. In addition to finding and  
91 categorizing the CH<sub>4</sub> enhancements (in a similar manner as done for the US cities in order to facilitate comparability), we  
92 made three additional measurements to better facilitate source attribution: the concomitant emission of ethane (C<sub>2</sub>H<sub>6</sub>) and CO<sub>2</sub>,  
93 and the carbon and hydrogen isotopic composition of the CH<sub>4</sub>. These tracers allow an empirically based source attribution for  
94 LIs. In addition to emission quantifications of LIs across the urban areas in these two cities, we also quantified CH<sub>4</sub> emissions  
95 from some of facilities within the municipal boundary of Utrecht and Hamburg using Gaussian plume dispersion model  
96 (GPDM).

## 97 **2 Materials and methods**

### 98 **2.1 Data collection and instrumentation**

#### 99 **2.1.1 Mobile measurements for attribution and quantification**

100 Mobile atmospheric measurements at street level were conducted using two Cavity Ring-Down Spectroscopy (CRDS)  
101 analyzers (Picarro Inc. model G2301 and G4302) which were installed on the back seat of a 2012 Volkswagen Transporter,  
102 (see supplementary information (SI), Sect. S.1.1, Figure S1). The model G2301 instrument provides atmospheric mole fraction  
103 measurements of CO<sub>2</sub>, CH<sub>4</sub> and H<sub>2</sub>O, each of them with an integration time of about 1 s., which results in a data frequency of  
104  $\approx 0.3$  Hz for each species. The reproducibility for CH<sub>4</sub> measurements was  $\approx 1$  ppb for 1 s integration time. The G2301  
105 instrument was powered by a 12 V car battery via a DC-to-AC converter. The flow rate was  $\approx 187$  ml min<sup>-1</sup>. Given the volume  
106 and pressure of the measurement cell (volume = 50 ml and pressure  $\approx 190$  mbar) the cell is flushed approximately every 3 s,  
107 so observed enhancements are considerably smoothed out. The factory settings for CH<sub>4</sub> and CO<sub>2</sub> were used for the water  
108 correction.

109 The G4302 instrument is a mobile analyzer that provides atmospheric mole fraction measurements of C<sub>2</sub>H<sub>6</sub>, CH<sub>4</sub>, and  
110 H<sub>2</sub>O. The flow rate is 2.2 L min<sup>-1</sup> and the volume of the cell is 35 ml (operated at 600 mb, thus 21 ml STP) so the cell is flushed  
111 in 0.01 s, which means that mixing is insignificant given the 1 s measurement frequency of the G4302. The additional  
112 measurement of C<sub>2</sub>H<sub>6</sub> is useful for source attribution since natural gas almost always contains a significant fraction of C<sub>2</sub>H<sub>6</sub>,  
113 whereas microbial sources generally do not emit C<sub>2</sub>H<sub>6</sub> (Yacovitch et al., 2014). The G4302 runs on a built-in battery which  
114 lasts for  $\approx 6$  h. The instrument can be operated in two modes at  $\approx 1$  Hz frequency for each species: the CH<sub>4</sub>-only mode and the  
115 CH<sub>4</sub> - C<sub>2</sub>H<sub>6</sub> mode. In the CH<sub>4</sub>-only mode the instrument has a reproducibility of  $\approx 10$  ppb for CH<sub>4</sub>. The factory settings for CH<sub>4</sub>  
116 and C<sub>2</sub>H<sub>6</sub> were used for the water correction. In the CH<sub>4</sub> - C<sub>2</sub>H<sub>6</sub> mode the reproducibility is about 100 ppb for CH<sub>4</sub> and 15 ppb  
117 for C<sub>2</sub>H<sub>6</sub>. For Utrecht surveys (see SI, Sect. S.1.2, Figure S2a), the G4302 was not yet available for the initial surveys in 2018,  
118 but it was added for the later re-visits (see SI, Sect. S.1.2, Table S1). For Hamburg (see SI, Sect. S.1.2, Figure S2b), both  
119 instruments operated during the entire intensive 3-week measurement campaign in Oct/Nov 2018 (see SI, Sect. S.1.2, Table  
120 S2). The time delay from the inlet to the instruments was measured and accounted for in the data processing procedure. The  
121 Coordinated Universal Time (UTC) time shifts between the Global Positioning System (GPS) and the two Picarro instruments

122 were corrected for each instrument in addition to the inlet delay (see SI, Sect. S.1.2, Table S1 and Table S2). The clocks on  
123 the Picarro instruments were set to UTC but showed drift over the period of the campaigns. We recorded the drifts for each  
124 day's survey and corrected to UTC time. The data were also corrected for the delay between air at the inlet and the signal in  
125 the CH<sub>4</sub> analyzers. This delay was determined by exposing the inlet to three small CH<sub>4</sub> pulses from exhaled breath, ranging  
126 from 5-30 seconds, depending on the instrument and tubing length. We averaged the three attempts to determine the delay for  
127 each instrument and used the delays for each instrument. Individual attempts were 1 to 2 s different from each other. For the  
128 G4302 the delay was generally about 5 s and for the G2301 it was about 30 s; the difference is mainly due to the different flow  
129 rates. The recorded CH<sub>4</sub> mole fractions were projected back along the driving track according to this delay.

130 One-quarter inch Teflon tubing was used to pull in air either from the front bumper (0.5 m above ground level) to the  
131 G2301 or from the rooftop (2 m above ground level) to the G4302. To avoid dust into the inlets for both instruments, Acrodisc®  
132 syringe filter, 0.2 µm was used for G2301 and Parker Balston 9933-05-DQ was used for G4302. The G2301 was used for  
133 quantification and attribution purposes and the G4302 mainly for attribution. After data quality check, a comparison between  
134 the two instruments during simultaneous measurements showed that all LIs were detectable by both instruments despite  
135 difference in inlet height (see SI, Sect. S.1.3, Figure S3). A comparison between the two instruments during simultaneous  
136 measurements showed that all LIs were detected by both instruments despite difference in instrument characteristics and inlet  
137 height. In the majority of cases CH<sub>4</sub> enhancements for each LI from both instruments were similar to each other. We note that  
138 there is likely a compensation of differences from two opposing effects between the two measurement systems. The inlet of  
139 the G2301 was at the bumper, thus closer to the surface sources, but the rather low flow rate and measurement rate of the  
140 instrument lead to some smoothing of the signal in the cavity. Because of the high gas flow rate, signal smoothing is much  
141 reduced for the G4302, but the inlet was on top of the car, thus further away from the surface sources (see Table S3 in SI, Sect.  
142 S.1.3). The vehicle locations were registered using a GPS system that recorded the precise driving track during each survey.

### 143 2.1.2 Target cities: Utrecht and Hamburg

144 Utrecht is the 4<sup>th</sup> largest city in the Netherlands with population of approximately 0.35 million inhabitants within an  
145 area of roughly 100 km<sup>2</sup>. It is located close to the center of the Netherlands and is an important infrastructural hub in the  
146 country. The Utrecht city area that we target in this study is well constrained by a ring of highways around the city (A27, A12,  
147 A2, and N230) with inhabitants of approximately 0.28 million living within this ring on roughly 45 km<sup>2</sup> of land. Figure S2a  
148 (see SI, Sect. S.1.2) shows the streets that were driven in Utrecht and Figure 1a shows the street coverage over four street  
149 categories (level 1, 2, 3, residential, and unclassified) obtained from the Open Street Map (OSM; [www.openstreetmap.org](http://www.openstreetmap.org)).  
150 Table S4 (see SI, Sect. S.1.5) provides information on road coverage based on different street categories. The hierarchy of  
151 OSM road classes is based on the importance of roads in connecting parts of the national infrastructure. Level 1 roads are  
152 primarily larger roads connecting cities, level 2 roads are the second most important roads and part of a greater network to  
153 connect smaller towns, level 3 roads have tertiary importance level and connect smaller settlements and districts. Residential  
154 roads are roads which connect houses and unclassified roads have the lowest importance of interconnecting infrastructure.  
155 Moreover, several transects were also made to measure the atmospheric mole fraction of CH<sub>4</sub> from the road next to the waste  
156 water treatment plant (WWTP) in Utrecht – a potentially larger single source of CH<sub>4</sub> emissions in the city (see SI, Sect. S.1.6,  
157 Table S5).

158 Hamburg is the 2<sup>nd</sup> largest city in Germany (about 1.9 million inhabitants, 760 km<sup>2</sup> area) and hosts one of the largest  
159 harbors in Europe. The study area in Hamburg is North of the Elbe river (Figure 1b) with ≈1.4 million inhabitants on about  
160 400 km<sup>2</sup> land. Figure S2b (see SI, Sect. S.1.2) shows the streets that were covered in Hamburg and Figure 1b shows the street  
161 coverage categorized in the four categories of OSM. More information on road coverage based on OSM street categories are  
162 provided in Table S4 (see SI, Sect. S.1.5). The local distribution companies (LDCs) in Utrecht (STEDIN

163 (<https://www.stedin.net/>) and Hamburg (GasNetz Hamburg (<https://www.gasnetz-hamburg.de>)) confirmed that full pipeline  
164 coverages are available beneath all streets. Therefore, the length of roads in the study area of Utrecht and Hamburg are  
165 representatives of NGDNs length. The Hamburg harbor area hosts several large industrial facilities that are related to the  
166 midstream / downstream oil and gas sector including refineries and storage tanks. An oil production site (oil well, separator  
167 and storage tanks) at Allermöhe (in Hamburg-Bergedorf) was also visited. Information from the State Authority for Mining,  
168 Energy and Geology (LBEG, 2018) was used to locate facilities. Precise locations of the facilities surveyed are given in the  
169 Table S6 (see SI, Sect. S.1.6). In order to separate these industrial activities from the NGDNs emissions in this study, CH<sub>4</sub>  
170 emissions from these locations were estimated, but evaluated apart from the emissions found in each city. The reported in-situ  
171 measurement, GPS data, and boundary of study areas reported here are available on the Integrated Carbon Observation System  
172 (ICOS) portal (Maazallahi et al., 2020b).

### 173 2.1.3 Driving strategy

174 The start/end point for each day's measurement surveys across Utrecht and Hamburg were the Institute for Marine  
175 and Atmospheric research Utrecht (IMAU; Utrecht University) and the Meteorological Institute (MI; Hamburg University),  
176 respectively. From these starting locations, each day's surveys targeted the different districts and neighborhoods of the cities  
177 (see SI, Sect. S.1.2, Table S1 and Table S2). Measurement time periods and survey areas were chosen to select favorable traffic  
178 and weather conditions and to avoid large events (e.g., construction; see SI, Sect. S.1.5, Figure S4), which normally took place  
179 between 10 - 18 LT. Average driving speeds on city streets were in the range of  $17 \pm 7$  km h<sup>-1</sup> in Utrecht and  $20 \pm 6$  km h<sup>-1</sup> in  
180 Hamburg.

181 As part of our driving strategy, we revisited locations where we had observed enhanced CH<sub>4</sub> readings (see SI, Sect.  
182 S.1.7, Figure S5). Not all recorded CH<sub>4</sub> mole fraction enhancements are necessarily the result of a stationary CH<sub>4</sub> source. For  
183 example, they could be related to emissions from vehicles which run on compressed natural gas, or vehicles operated with  
184 traditional fuels but with faulty catalytic converter systems. Later we will discuss how to exclude or categorize these  
185 unintended signals (see Sect. 2.2.2 and Sect. 2.3.1). Therefore, we revisited a large number of locations (65 in Utrecht ( $\approx 80$   
186 %) and 100 in Hamburg ( $\approx 70$  %)) where enhanced CH<sub>4</sub> had been observed in during the first survey in order to confirm the  
187 LIs. In contrast to the measurements carried out in many cities in the United States (US) (von Fischer et al., 2017), our  
188 measurements were not carried out using Google Street View cars, but with a vehicle from the Institute for Marine and  
189 Atmospheric research Utrecht (IMAU), Utrecht University (see SI, Sect. S.1.1, Figure S1). Due to time and budget restrictions,  
190 it was not possible to cover each street at least twice, as done for the US cities. After evaluation of the untargeted first surveys  
191 that covered each street at least once, targeted surveys were carried out for verification of observed LIs and for collection of  
192 air samples at locations with high CH<sub>4</sub> enhancements. The rationale behind this measurement strategy is that if an enhancement  
193 was not recorded during the first survey, it obviously cannot be verified in the second survey. The implications of the difference  
194 in the measurement strategy will be discussed in the Results and Discussion sections below.

195 In total, approximately 1,300 km of roads were driven during Utrecht surveys and about 2,500 km during the Hamburg  
196 campaign. In Utrecht, some re-visits were carried out several months to a year after the initial surveys in order to check on the  
197 persistence of the LIs. In Hamburg, revisits were also performed within the 4-week intensive measurement period. Further  
198 details about the driving logistics are provided in the SI (Sect. S.1.6, Table S1 and Table S2). It is possible that pipeline leaks  
199 that were detected during the initial survey were repaired before the revisit, and the chance of this occurring increases as the  
200 time interval between visits gets longer.

## 201 2.1.4 Air sample collection for attribution

202 In addition to the mobile measurement of C<sub>2</sub>H<sub>6</sub> and CO<sub>2</sub> for LIs attributions purposes, samples for lab isotope analysis  
203 of δ<sup>13</sup>C-CH<sub>4</sub> and δ<sup>2</sup>H-CH<sub>4</sub> (hereinafter δ<sup>13</sup>C and δD respectively) were collected during the revisits at locations that had  
204 displayed high CH<sub>4</sub> enhancements during the first surveys. Depending on the accessibility and traffic, samples were either  
205 taken inside the car (see SI, Sect. S.1.8, Figure S6a) using a tubing from the bumper inlet, or outside the car on foot using the  
206 readings from the G4302 to find the best location within the plume (see SI, Sect. S.1.8, Figure S6b). All the samples taken in  
207 the North Elbe study area and from most of the facilities were collected when the car was parked, but the samples inside the  
208 New Elbe tunnel and close to some facilities where there was no possibility to park were taken in motion while we were within  
209 the plume. The sampling locations across the North Elbe study area of Hamburg were determined based the untargeted surveys,  
210 and the confirmation during revisits. The C<sub>2</sub>H<sub>6</sub> information was not used in the selection of sampling locations in order to  
211 avoid biased sampling. Sampling locations from the facilities were determined based on wind direction, traffic, and types of  
212 different activities. Samples for isotope analysis were collected in non-transparent aluminum-coated Tedlar Supelco, Seupel™  
213 Inert SCV Gas Sampling Bag (2 L) and SKC, Standard FlexFoil® Air Sample Bags (3 L) using a 12 V pump and 1/4-inch  
214 Teflon tubing which pumps air with flow rate of ≈0.25 L min<sup>-1</sup>. In total, 103 bag samples were collected at 24 locations in  
215 Hamburg, 14 of them in the city area North of the Elbe river and 10 at larger facilities. Usually, three individual samples were  
216 collected at each source location, plus several background air samples on each sampling day. This sampling scheme generally  
217 results in a range of mole fractions that allow source identification using a Keeling plot analysis (Keeling, 1958, 1961). Fossil  
218 CH<sub>4</sub> sources in the study areas of this paper (inside the ring for Utrecht and north Elbe in Hamburg) refers to emissions  
219 originating from natural gas leaks.

## 220 2.1.5 Meteorological Data

221 Meteorological information reflecting the large scale wind conditions during the campaigns were obtained from  
222 measurements at the Cabauw tower (51.970263° N, 4.926267° E) operated by Koninklijk Nederlands Meteorologisch Instituut  
223 (KNMI) (Van Ulden and Wieringa, 1996) for Utrecht and Billwerder tower (53.5192° N, 10.1029° E) operated by the MI at  
224 Hamburg University (Brümmer et al., 2012) for Hamburg. The wind direction and wind speed data from the masts were used  
225 for planning the surveys. Pressure and temperature measurements were used to convert volume to mass fluxes for CH<sub>4</sub>. We  
226 also used information from the towers for the GPDM calculations of the emission rates from larger facilities, because the local  
227 wind measurements from the 2-D anemometer were not logged continuously due to failure in logging setup of the  
228 measurements. In Utrecht, the Cabauw tower is located about 20 km from the WWTP. In Hamburg Billwerder tower is about  
229 18 km from the Soil and Compost company and about 8 km from oil production facilities. Uncertainties over the wind data  
230 will be described later.

## 231 2.2 Emission quantification

### 232 2.2.1 Data preparation and background extraction of mobile measurements

233 The first step of the evaluation procedure is quality control of the data from both CH<sub>4</sub> analyzers and the GPS records.  
234 Periods of instrument malfunction and unintended signals based on notes written during each day's measurements were  
235 removed from the raw data. Extraction of the LIs from in-situ measurements requires estimation of the background levels (see  
236 SI, Sect. S.2.1, Figure S7). We estimated CH<sub>4</sub> background as the median value of ± 2.5 min of measurements around each  
237 individual point as suggested in Weller et al. (2019). For estimating the CO<sub>2</sub> background level we used the 5<sup>th</sup> percentile of ±  
238 2.5 min of measurements around each individual point (Brantley et al., 2014; Bukowiecki et al., 2002). The background  
239 determination method for CH<sub>4</sub> was selected from Weller et al. (2019) to follow the emission quantification algorithm for the

240 urban studies, and while this algorithm doesn't include background extraction for CO<sub>2</sub>, we chose commonly adopted method  
241 of background determination for this component. These background signals were subtracted from the measurement time series  
242 to calculate the CH<sub>4</sub> and CO<sub>2</sub> enhancements. For C<sub>2</sub>H<sub>6</sub>, the background was considered zero as it is normally present at a very  
243 low mole fraction; between ~0.4-2.5 ppb (Helmig et al., 2016), and is lower than the G4302 detection limit.

## 244 2.2.2 Quantification of methane emissions from leak indications

245 We wrote an automated MATLAB<sup>®</sup> script (available on GitHub from Maazallahi et al. (2020a)) based on the  
246 approach initially introduced in von Fischer et al. (2017), and improved in Weller et al. (2019). This algorithm was designed  
247 to quantify CH<sub>4</sub> emissions from ground-level emission release locations within 5-40 m from the measurement (von Fischer et  
248 al., 2017), such as pipeline leaks and has been demonstrated that the algorithm adequately estimates the majority of those  
249 emissions from a city (Weller et al., 2018). Using the same algorithm also ensures that results are comparable between  
250 European and US cities. The individual steps will be described below. Mapping and spatial analysis were conducted using  
251 Google Earth and ESRI ArcMap software. A flow diagram of the evaluation procedure is provided in the SI (Sect. S.2.2, Figure  
252 S8).

253 Following the algorithm from von Fischer et al. (2017), measurements at speeds above 70 km h<sup>-1</sup> were excluded, as  
254 the data from the controlled release experiments (von Fischer et al., 2017) were not reliable at high speed (Weller et al., 2019).  
255 We also excluded measurements during periods of zero speed (stationary vehicle) to avoid unintended signals coming from  
256 other cars running on compressed natural gas when the measurement car was stopped in traffic. In order to merge the sharp 1  
257 Hz-frequency records of the GPS with the ≈ 0.3 Hz data from the G2301 analyzer, the CH<sub>4</sub> mole fractions were linearly  
258 interpolated to the GPS times.

259 Weller et al., (2019) established an empirical equation to convert LIs observed with a Picarro G2301 in a moving  
260 vehicle in urban environments into emission rates based on a large number of controlled release experiments in various  
261 environments (Eq. (1)).

$$262 \ln(C) = -0.988 + 0.817 * \ln(Q) \quad (1)$$

263 In this equation, C represents CH<sub>4</sub> enhancements above the background in ppm and Q is the emission rate in L min<sup>-1</sup>  
264 <sup>1</sup>. Weller et al., (2019) used controlled releases to demonstrate that the magnitude of the observed methane enhancement is  
265 related to the emission rate and carefully characterized the limitations and associated errors of this equation. We used Eq. (1)  
266 to convert CH<sub>4</sub> enhancements encountered during our measurements in Utrecht and Hamburg to emission rates, and we use  
267 these estimates to categorize LIs into three classes: high (emission rate > 40 L min<sup>-1</sup>), medium (emission rate 6– 40 L min<sup>-1</sup>)  
268 and low (emission rate 0.5 - 6 L min<sup>-1</sup>), following the categories from von Fischer et al. (2017) (Table 1).

269 The spatial extent of individual LIs was estimated as the distance between the location where the CH<sub>4</sub> mole fraction  
270 exceeded the background by more than 10 % (≈ 0.200 ppm; as used in von Fischer et al. (2017) and Weller et al. (2019)) to  
271 the location where it fell below this threshold level again. LIs which stay above the threshold for more than 160 m were  
272 excluded in the automated evaluation because we suspect that such extended enhancements are most likely not related to leaks  
273 from the NGDN (von Fischer et al., 2017).

274 In a continuous measurement survey on a single day, consecutive CH<sub>4</sub> enhancements above background observed  
275 within 5 seconds were aggregated and the location of the emission source was estimated based on the weighted averaging of  
276 coordinates (Eq. (2)). Decimal degree coordinates were converted to Cartesian coordinates (see SI, Sect. S.2.3, Figure S9)  
277 relative to local references (see SI, Sect. S.2.3, Table S7). In Utrecht, the Cathedral tower (Domtoren) and in Hamburg the St.  
278 Nicholas' Church were selected as local geographic datums. LIs observed on different days at similar locations were clustered  
279 and interpreted as one point source when circles of 30 m radius around the centre locations overlapped, similar to Weller et  
280 al., (2019). The enhancement of the cluster was assigned the maximum observed mole fraction and located as the weighted

281 average of the geographical coordinates of the LIs within that cluster (Eq. (2) from Weller et al. (2019)), where  $w_i$  is CH<sub>4</sub>  
282 enhancement of each LI.

$$283 \text{ (lon, lat)} = \frac{\sum_{i=1}^n w_i * (\text{lon}_i, \text{lat}_i)}{\sum_{i=1}^n w_i} \quad (2)$$

284 We compared the outputs of our software to the one developed by Colorado State University (CSU) for the surveys  
285 in US cities (von Fischer et al., 2017; Weller et al., 2019). 30 LIs were detected and no significant differences were observed  
286 (linear fit equation  $y = 1.00 * x - 0.00$ ,  $R^2 = 0.99$ ) (see SI, Sect. S.2.4, Figure S10). As mentioned above, in our campaign-type  
287 studies not all streets were visited twice, so this criterion was dropped from the CSU algorithm. Instead, we used explicit  
288 source attribution by co-emitted tracers.

289 The emission rate per km of road covered during our measurements was then scaled up to the city scale using the  
290 ratio of total road length within the study area boundaries derived from OSM to the length of streets covered, and converted  
291 to a per-capita emission using the population in the study areas based on LandScan data (Bright et al., 2000). Note that in this  
292 up-scaling practice, emission quantified from facilities were excluded.

293 To account for the emission uncertainty, similar to Weller et al. (2018) for the US city studies, we used a bootstrap  
294 technique which was initially introduced in Efron (1979, 1982), as this technique is adequate in resampling of both parametric  
295 and non-parametric problems with even non-normal distribution of observed data. Tong et al. (2012) indicated that bootstrap  
296 resampling technique is sufficiently capable in estimating uncertainty of emissions with sample size of equal or larger than 9.  
297 Efron and Tibshirani (1993) suggested that minimum of 1,000 iterations are adequate in bootstrap technique. In this study, we  
298 used non-parametric bootstrap technique to account for the uncertainty of total CH<sub>4</sub> emissions from all LIs in each city with  
299 30,000 replications. As mentioned above the algorithm is based on CH<sub>4</sub> enhancements of measurement with 5-40 m distance  
300 from controlled release location, and can produce large uncertainty for emission quantification of individual LI (Figure 4 in  
301 Weller et al. (2019)), but with sufficient number of sample size, the uncertainty associated with total emission quantified in an  
302 urban area is more precise.

### 303 2.2.3 Quantification of methane emissions from larger facilities

304 Apart from the natural gas distribution network, there are larger facilities in both cities that are potential CH<sub>4</sub> sources  
305 within the study area. Several facilities in or around the cities were visited during the mobile surveys to provide emission  
306 estimates. We applied a standard point source GPDM (Turner, 1969) to quantify methane emissions from these larger facilities.  
307 A flowchart describing the steps taken during quantification from facilities is given in SI (Sect. S.2.5., Figure S11). We note  
308 that emission quantification using GPDM with data from mobile measurements is prone to large errors (factor of 3 or more )  
309 (Yacovitch et al., 2018) especially when the measurements are carried out close to the source. In this study, we also report the  
310 data obtained from larger facilities, since rough emission estimates from facilities can be obtained in the city surveys. Caulton  
311 et al. (2018) discuss uncertainties of emission quantification with GPDM. Individual facilities were visited during the routine  
312 screening measurements and during revisits for LI confirmation and air sampling.

313 In Utrecht, the WWTP is located in the study area and streets around this facility were passed several times during  
314 surveys. In Hamburg, we initially performed screening measurements in the harbor area (extensive industrial activities) and  
315 near an oil production site and then revisited these sites for further quantification and isotopic characterization. The data from  
316 the oil production site can be fit reasonably well with a GPDM and were therefore selected for quantification, similar to studies  
317 in a shale gas production basin in the USA (Yacovitch et al., 2015) and in the Netherlands (Yacovitch et al., 2018).

$$318 C(x, y, z) = \frac{Q}{2 * \pi * u * \sigma_y * \sigma_z} * \left\{ \exp\left(\frac{-(z - z_{source})^2}{2 * \sigma_z^2}\right) + \exp\left(\frac{-(z + z_{source})^2}{2 * \sigma_z^2}\right) \right\} * \exp\left(\frac{-y^2}{2 * \sigma_y^2}\right)$$

319 (3)

320 In Eq. (3), C is the CH<sub>4</sub> enhancement converted to the unit of g/m<sup>3</sup> at cartesian coordinates x, y, and z relative to the  
321 source ([x y z]<sub>source</sub> = 0), x is the distance of the plume from the source aligned with the wind direction, y is the horizontal axis



322 perpendicular to the wind direction,  $z$  is the vertical axis.  $Q$  is emission rate in  $\text{g s}^{-1}$ ,  $u$  ( $\text{m s}^{-1}$ ) is the wind speed along the  $x$ -  
323 axis, and  $\sigma_y$  and  $\sigma_z$  are the horizontal and vertical plume dispersion parameters (described below), respectively.

324 Determination of an effective release location is a challenge for the larger facilities. Effective emission locations for  
325 each facility were estimated based on wind direction measurements and the locations of maximum  $\text{CH}_4$  enhancements. The  
326 facilities were generally visited multiple times under different wind conditions. The locations of the maximum  $\text{CH}_4$   
327 enhancements were then projected against the ambient wind, and the intersection point of these projections during different  
328 wind conditions was defined as effective emission location of the facility. At least two measurement transects with different  
329 wind direction were used to estimate the effective location of the source. If wind directions, road accessibility or the shape of  
330 plumes were not sufficient to indicate the effective source location, the geographical coordinates of centroids of the possible  
331 sources using Google Earth imageries and field observations were used to determine the effective emission location. For the  
332 WWTP in Utrecht we also contacted the operator and asked for the location of sludge treatment as it is the major source of  
333  $\text{CH}_4$  emissions (Paredes et al., 2019; Schaum et al., 2015).

334 Neumann and Halbritter (1980) showed that the main parameters in sensitivity analysis of GPDM are the wind speed  
335 and source emission height in close distance and the influence of emission height become less further downwind compared to  
336 the mixing layer height. In this study, the heights of emission sources were low ( $<10\text{m}$ ) and estimated during surveys and/or  
337 using Google Earth imageries, and considering that such a larger measurement distance from the facilities, the main sources  
338 of uncertainty of the emission estimates for the WWTP and Compost and Soil company are most likely the mean wind speed  
339 and for the upstream facilities in Hamburg the major sources of uncertainties can be the mean wind speed and emission height.  
340 We considered 0-4 m source height for the WWTP in Utrecht, and for the upstream facilities in Hamburg we considered 0-5  
341 m emission height for the Compost and Soil site, 0-2 m for the separator, 0-10 m for the storage tank, and 0-1 m for the oil  
342 extraction well-head. We used 1 m interval for each of these height ranges to quantify emissions in GPDM.

343 Cross wind horizontal dispersions  $\sigma_y$  were estimated from the measured plumes by fitting a Gaussian curve to the  
344 individual plumes from each set during each day's survey. A set of plumes is defined as a back to back transects during a  
345 period of time downwind each facility on different days. Later average emissions from all sets of plumes were used to report  
346  $\text{CH}_4$  emission for each of the facilities. A suitable Pasquill–Gifford stability class was then determined by selecting a pair of  
347 parameters (Table 1-1 in EPA, 1995) that matches best and give the closest number to the with the fitted value of  $\sigma_y$ . Vertical  
348 dispersions  $\sigma_z$  were then estimated using the identified Pasquill–Gifford stability class in the first step, using the distances to  
349 the source locations (Table 1-2 in EPA, 1995). Uncertainties due to these estimates will be discussed below. Mass emission  
350 rates were calculated using the metric volume of  $\text{CH}_4$  at 1 bar of atmospheric pressure ( $0.715 \text{ kg m}^{-3}$  at  $0^\circ\text{C}$  and  $0.666 \text{ kg m}^{-3}$   
351 at  $20^\circ\text{C}$ , P. 1.124 in IPCC, 1996), and linear interpolation was used for temperatures in between.

352 Due to technical issues, local wind data were not logged continuously and thus we used wind data from two towers  
353 which are 8 to 20 km away from the facilities we focused for emission quantifications. These distances introduce extra  
354 uncertainties in analyzing the emissions using GPDM mainly on the wind speed. By comparing some of the local high-quality  
355 wind data to data from the towers, we estimated that the local wind speed is within the range of  $\pm 30\%$  of the collected tower  
356 data. This range was adopted to estimate the wind speed for emission quantifications for the set of plumes measured downwind  
357 of the facilities. The wind directions were aligned at local scale of each facility based on the locations of sources and locations  
358 of maxima of average  $\text{CH}_4$  enhancements from a set of transects in each day's survey and we considered  $\pm 5^\circ$  uncertainty in  
359 wind direction for the GPDM quantification.

## 360 2.3 Emission attribution

### 361 2.3.1 Mobile C<sub>2</sub>H<sub>6</sub> and CO<sub>2</sub> measurements

362 During the Utrecht campaign, the overall mole fraction of CH<sub>4</sub> and C<sub>2</sub>H<sub>6</sub> in the NGDN was  $\approx 80\%$  and  $\approx 3.9\%$   
363 (STEDIN, personal communication) and in Hamburg the mole fraction of CH<sub>4</sub> and C<sub>2</sub>H<sub>6</sub> in the NGDN was about  $\approx 95\%$  and  
364  $\approx 3.4\%$  (GasNetz Hamburg, personal communication) respectively. This ratio can vary depending on the mixture of gas  
365 compositions from different suppliers, but should meet the standards on the gas compositions in the Netherlands (65 – 96 mol-  
366 % for CH<sub>4</sub> and 0.2 – 11 mol-% for C<sub>2</sub>H<sub>6</sub> (ACM, 2018)) and in Germany (83.64 – 96.96 mol-% for CH<sub>4</sub> and 1.06 – 6.93 mol-  
367 % for C<sub>2</sub>H<sub>6</sub> (DVGW, 2013)). Compressed natural gas vehicles can be mobile CH<sub>4</sub> emission sources ( E. K. Nam et al., 2004;  
368 Curran et al., 2014; Naus et al., 2018; Popa et al., 2014) and in this study we also observed CH<sub>4</sub> signals from vehicles. For  
369 example, the point to point C<sub>2</sub>H<sub>6</sub>:CH<sub>4</sub> ratio (C<sub>2</sub>:C<sub>1</sub>) calculated from road measurements of a car exhaust shown in Figure S12  
370 (see SI, Sect. S.2.6) is  $14.2 \pm 7.1\%$ . During the campaigns in Utrecht and Hamburg the C<sub>2</sub>:C<sub>1</sub> of NGDNs was less than 10 %  
371 and in our study, we removed all the locations where the C<sub>2</sub>:C<sub>1</sub> ratio was greater than 10 %. CH<sub>4</sub> emissions from combustion  
372 processes are always accompanied by large emissions of CO<sub>2</sub> and can therefore be identified based on the low CH<sub>4</sub>:CO<sub>2</sub>  
373 emission ratio. In this study, LIs with CH<sub>4</sub>:CO<sub>2</sub> ratio between 0.02 and 20 with R<sup>2</sup> greater than 0.8 were attributed to  
374 combustion.

### 375 2.3.2 Lab isotopic analysis of $\delta^{13}\text{C}$ and $\delta\text{D}$

376 After sample collections, the bag samples were returned to the IMAU for analysis of both  $\delta^{13}\text{C}$  and  $\delta\text{D}$  (Brass and  
377 Röckmann, 2010) and some samples were analyzed at the Greenhouse Gas Laboratory (GGL) in the department of Earth  
378 Sciences, Royal Holloway University of London (RHUL) for  $\delta^{13}\text{C}$  (Fisher et al., 2006) (see SI, Sect. S.2.7, Figure S13).

379 At the IMAU, we used isotope ratio mass spectrometry (IRMS) instrument of ThermoFinnigan MAT DeltaPlus XL  
380 (Thermo Fisher Scientific Inc., Germany). We used a reference cylinder calibrated against Vienna Pee Dee Belmnite (V-PDB)  
381 for  $\delta^{13}\text{C}$  and Vienna Standard Mean Ocean Water (V-SMOW) for  $\delta\text{D}$  at the at the Max Planck Institute for Biogeochemistry  
382 (MPI-BGC), Jena, Germany (Sperlich et al., 2016). The cylinder contained CH<sub>4</sub> mole fraction of  $1975.5 \pm 6.3$  ppb,  $\delta^{13}\text{C} = -$   
383  $48.14 \pm 0.07\%$  vs V-PDB and  $\delta\text{D} = -90.81 \pm 2.7\%$  vs V-SMOW. The samples were pumped through a magnesium perchlorate  
384 (Mg(ClO<sub>4</sub>)<sub>2</sub>) dryer before the CH<sub>4</sub> extraction steps. Each sample was measured at least 2 times (up to four times) for each  
385 isotope. Every other sample, the reference gas was also measured 3 times for  $\delta^{13}\text{C}$  and  $\delta\text{D}$ . Each measurement, from the CH<sub>4</sub>  
386 extraction to the mass spectrometer, took  $\approx 30$  minutes.

387 At the GGL, Flex foil SKC bag samples were each analyzed for methane mole fractions and  $\delta^{13}\text{C}$ . Methane mole  
388 fractions were determined using a Picarro G1301 CRDS, which measured every 5 seconds for 2 minutes resulting in a precision  
389  $\pm 0.3$  ppb (Lowry et al., 2020; France et al., 2016; Zazzeri et al., 2015). Each sample was then measured for stable isotopes  
390 ( $\delta^{13}\text{C}$ -CH<sub>4</sub>) using an Elementar Trace gas and continuous-flow gas chromatography isotope ratio mass spectrometry (CF-GC-  
391 IRMS) system (Fisher et al., 2006), which has an average repeatability of  $\pm 0.05\%$ . CH<sub>4</sub> extraction was preceded by drying  
392 process using Mg(ClO<sub>4</sub>)<sub>2</sub>. Each sample was measured 3 times for  $\delta^{13}\text{C}$ -CH<sub>4</sub>, where the duration of each analysis was  $\approx 20$   
393 minutes. Both instruments are calibrated weekly to the WMO X2004A methane scale using air filled cylinders that were  
394 measured by the National Oceanic and Atmospheric Administration (NOAA), and cylinders that were calibrated against the  
395 NOAA scale by the MPI-BGC (France et al., 2016; Lowry et al., 2020).

396 The analytical systems for isotope analysis have been described, used and/or compared in several previous  
397 publications (Fisher et al., 2011; Röckmann et al., 2016; Umezawa et al., 2018; Zazzeri et al., 2015). Measurement  
398 uncertainties in  $\delta^{13}\text{C}$  and  $\delta\text{D}$  are 0.05-0.1 % and 2-5 % respectively.

399 After the LIs were analyzed and quantified, the measurements of C<sub>2</sub>H<sub>6</sub>, CO<sub>2</sub>, and isotopic composition from the air  
400 samples were used for source attribution. We characterize the observed LIs as of fossil origin when they had a concomitant  
401 C<sub>2</sub>H<sub>6</sub> signal between 1 % and 10 % of the CH<sub>4</sub> enhancements and when the isotopic composition was in the range -50 to -40  
402 ‰ for δ<sup>13</sup>C and -150 to -200 ‰ for δD. A LI was characterized as microbial when there was no C<sub>2</sub>H<sub>6</sub> signal (<1 % of the CH<sub>4</sub>  
403 enhancements larger than 500 ppb), δ<sup>13</sup>C was between -55 ‰ and -70 ‰ and δD was between -260 and -360 ‰ (Figure 7 in  
404 Röckmann et al., 2016). LIs with enhancements of CH<sub>4</sub> lower than 500 ppb and no C<sub>2</sub>H<sub>6</sub> signals were categorized as  
405 unclassified. LIs with no C<sub>2</sub>H<sub>6</sub> signals, no significant CH<sub>4</sub>:CO<sub>2</sub> ratio, and no information on δ<sup>13</sup>C and δD were also categorized  
406 as unclassified. The source signatures for each sampling location were determined by a Keeling plot analysis of the three  
407 samples collected in the plumes and a background sample taken on the same day.

## 408 3 Results

### 409 3.1 Quantification of CH<sub>4</sub> emissions across Utrecht and Hamburg

410 Table 2 summarizes the main results from the surveys in Hamburg and Utrecht. The amount of km of roads covered  
411 in Hamburg is roughly a factor of 2 larger than in Utrecht, and also the number of detected LIs is roughly a factor of 2 larger,  
412 for all three categories. This shows that the overall density of LIs (km covered per LI) in both cities is not very different.  
413 Specifically, a LI is observed every 5.6 km in Utrecht and every 8.4 km in Hamburg. While not all streets were visited twice  
414 in both cities (see SI, Sect. S.1.5, Table S4) 80 % of LIs in Utrecht and 69 % of LIs in Hamburg were revisited which account  
415 for 91 % and 86 % of emissions respectively in the study areas. During revisits, 60 % of CH<sub>4</sub> emissions in Utrecht and 46 %  
416 of emissions in Hamburg were confirmed. In both cities, all LIs in the high emission category were re-observed. In some cases,  
417 re-visits were carried out several months after first detection, and the LIs were still confirmed (e.g. see SI, Sect. S.1.7, Figure  
418 S5).

419 The distribution of CH<sub>4</sub> LIs across the cities of Utrecht and Hamburg is shown in Figure 2. As shown in Table 2, a  
420 total of 145 significant LIs were detected in Hamburg and 81 in Utrecht; these LIs cover all three LI categories. Two LIs in  
421 Hamburg and one LI in Utrecht fall in the high (red) emission category; the highest LI detected in Utrecht and Hamburg  
422 corresponded to emission rates of  $\approx 100 \text{ L min}^{-1}$  and  $\approx 70 \text{ L min}^{-1}$ , respectively. Noted that estimates for individual leaks with  
423 the Weller et al. (2019) algorithm can have large error, thus these results are indicative of large leaks, but the precise emission  
424 strength is very uncertain. Six LIs in Utrecht and 16 LIs in Hamburg fall in the middle (orange) emission category, and 127  
425 LIs in Hamburg and 74 LIs in Utrecht fall in the low (yellow) emission category. The distribution of emissions over the three  
426 categories is also similar between the two cities, with roughly one third of the emissions originating from each category (Figure  
427 2), but the number of LIs in each category is different. The contribution of LIs in the high emission category is about a third  
428 of the total observed emissions (35 % in Utrecht is (1 LI) and in 30 % in Hamburg (2 LIs)).

429 CH<sub>4</sub> emitting locations were categorized based on the roads where the LIs were observed (Figure 1, Figure 2, Figure  
430 3, and Table S8 in SI, Sect. S.3.1). Average emission rates per LI as derived from equation (1) are similar for the two cities  
431 with  $3.6 \text{ L min}^{-1} \text{ LI}^{-1}$  in Utrecht and  $3.4 \text{ L min}^{-1} \text{ LI}^{-1}$  in Hamburg, but they are distributed differently across the road (Figure  
432 1). In Utrecht, emitting locations on level 2 roads contributed the most (50 % of emissions) to the total emissions while in  
433 Hamburg the majority of the emissions occurred on residential roads (56 % of total emissions). This shows that the major leak  
434 indications may happen on different road classes in different cities and there is no general relation to the size of streets between  
435 these two cities.

436 In Figure 4, we compare cumulative CH<sub>4</sub> emissions for Utrecht and Hamburg to numerous US cities (Weller et al., 2019).  
437 After ranking the LIs from largest to smallest, it becomes evident that the largest 5 % of the LIs account for about 60 % of  
438 emissions in Utrecht, and 50 % of the emissions in Hamburg.

439 As mentioned above, the observed total emission rates observed on roads in urban environment in the two cities are  
440 relatively similar when normalized by the total amount of km covered, 0.64 L min<sup>-1</sup> km<sup>-1</sup> for Utrecht and 0.4 L min<sup>-1</sup> km<sup>-1</sup> for  
441 Hamburg (Table 2). Using these two emission factors, the observed emission rates ( $\approx 110$  t yr<sup>-1</sup> in Utrecht and  $\approx 180$  t yr<sup>-1</sup> in  
442 Hamburg) were up-scaled to the entire road network in the two cities,  $\approx 650$  km in Utrecht and  $\approx 3,000$  km in Hamburg. This  
443 includes the implicit assumption that the pipeline network is similar to the street network. Total up-scaled emission rates based  
444 on mobile measurements on roads in urban environment before considering attribution analysis over LI locations are 150 t yr<sup>-1</sup>  
445 and 440 t yr<sup>-1</sup> across the study areas of Utrecht and Hamburg respectively. Distributing the calculated emission rates over the  
446 population in the city areas yields emission rates of  $0.54 \pm 0.15$  kg yr<sup>-1</sup> capita<sup>-1</sup> for Utrecht and  $0.31 \pm 0.04$  kg yr<sup>-1</sup> capita<sup>-1</sup> for  
447 Hamburg (see SI, Sect. S.3.2, Figure S14).

### 448 3.2 Attribution of CH<sub>4</sub> emissions across Utrecht and Hamburg

449 Figure 5 shows the results of the isotope analysis for the 21 locations in Hamburg where acceptable Keeling plots  
450 were obtained (see SI, Sect. S.3.3, Table S9 and Table S10). The results cluster mostly in three groups, which are characterized  
451 by the expected isotope signatures for fossil, microbial, and pyrogenic samples as described in Röckmann et al., (2016).

452 Average isotope signatures for the LIs in the city of Hamburg were  $\delta^{13}\text{C} = -52.3 \pm 5.1$  ‰ and  $\delta\text{D} = -298.4 \pm 30.3$  ‰  
453 for the samples characterized as microbial and  $\delta^{13}\text{C} = -41.9 \pm 1.0$  ‰ and  $\delta\text{D} = -196.1 \pm 10.6$  ‰ for the samples characterized  
454 as fossil (Figure 5). One sample from the Hamburg city area displays a very high source signature of  $\delta^{13}\text{C} = -23$  ‰ and  $\delta\text{D} =$   
455  $-153$  ‰. The origin of CH<sub>4</sub> with such an unusual isotopic signature could not be identified and it is considered an outlier. In  
456 Hamburg, 10 % of the LI locations (38 % of emissions) on the north side of Elbe were sampled for isotope analysis. The lab  
457 isotopic attributions show that the LIs with the higher emission rates are mostly caused by emission of fossil CH<sub>4</sub>. 79 % of the  
458 inferred emissions at 38 % of the LIs were identified as of fossil origin, 20 % of emissions at 54 % of the LIs as of microbial  
459 origin (for an identified source see SI, Sect. S.3.3, Figure S15), 1 % of emissions at 8 % of LIs as of pyrogenic origin.

460 In Hamburg, during three passes through the new Elbe tunnel (see SI, Sect. S.3.4, Figure S16) a CH<sub>4</sub>:CO<sub>2</sub> of  $0.2 \pm$   
461  $0.1$  ppb:ppm was derived for combustion-related emission. During the surveys of open roads, clear CH<sub>4</sub>:CO<sub>2</sub> correlations were  
462 observed for several LIs and an example of a measurement of car exhaust is shown in Figure S12a (see SI, Sect. S.2.6) with  
463 CH<sub>4</sub>:CO<sub>2</sub> = 1.6 ppb:ppm. Previous studies have shown relatively low CH<sub>4</sub>:CO<sub>2</sub> ratios of  $4.6 \cdot 10^{-2}$  ppb:ppm (Popa et al., 2014),  
464 0.41 ppb ppm<sup>-1</sup> (E. K. Nam et al., 2004), and 0.3 ppb:ppm (Naus et al., 2018) when cars work under normal conditions. During  
465 cold engine (Naus et al., 2018) or incomplete combustion conditions, the fuel to air ratio is too high, which results in enhanced  
466 emission of black carbon particles and reduced carbon compounds, so higher CH<sub>4</sub>:CO<sub>2</sub> ratios. Hu et al. (2018) reported  $2 \pm 2.1$   
467 ppb:ppm in a tunnel, but  $12 \pm 5.3$  ppb:ppm<sup>1</sup> on roads. In addition to car exhaust, there are other combustion sources which  
468 can affect CH<sub>4</sub> and CO<sub>2</sub> mole fractions at the street level including natural gas water heater (CH<sub>4</sub>:CO<sub>2</sub> ratio of  $\approx 2$  ppb:ppm;  
469 Lebel et al., 2020), restaurant kitchens, etc. Based on the CH<sub>4</sub>:CO<sub>2</sub> ratio (ppb:ppm) criterion defined above (see Sect. 2.3.1),  
470 17 % of LIs (10 % of emissions) can be attributed to combustion (see SI, Sect. S.3.4, Figure S17) with a mean CH<sub>4</sub>:CO<sub>2</sub> ratio  
471 of  $3.2 \pm 3.9$  ppb:ppm (max = 18.7 and min = 0.8 ppb:ppm). The C<sub>2</sub>:C<sub>1</sub> ratio for these LIs attributed to combustion in Hamburg  
472 was  $7.8 \pm 3.5$  %. In Utrecht 7 % of LIs (2 % of emissions) are attributed to combustion with a mean CH<sub>4</sub>:CO<sub>2</sub> ratio of  $9.8 \pm$   
473  $5.8$  ppb:ppm (max = 16.7 and min = 3.0 ppb:ppm).

474 Based on the C<sub>2</sub>H<sub>6</sub> signals, 64 % of the emissions (33 % of LIs) were characterized as fossil, while 25 % of emissions  
475 (20 % of LIs) were identified as microbial. Due to low CH<sub>4</sub> and C<sub>2</sub>H<sub>6</sub> enhancements, 47 % of the locations (11 % of emission)  
476 were considered unclassified. The C<sub>2</sub>:C<sub>1</sub> ratio for the LIs attributed to emissions from NGDNs in Hamburg study area (North  
477 Elbe) is  $4.1 \pm 2.0$  %. The oil production site in south-east Hamburg had a higher C<sub>2</sub>:C<sub>1</sub> ratio of  $7.1 \pm 1.5$  %.

478 In Utrecht, C<sub>2</sub>H<sub>6</sub> was measured only during four surveys in February, April, and June 2019 (revisits of 2-day surveys  
479 across the city center and 2 days to LIs with high emission rates) as the CH<sub>4</sub> - C<sub>2</sub>H<sub>6</sub> analyzer was not available during the first

480 campaign. The C<sub>2</sub>:C<sub>1</sub> ratios from this limited survey indicates that 93 % of emissions (69 % of the LIs across the city centre,  
481 including combustions) are likely from fossil sources (Table 2) and 73 % of emissions (43 % of the LIs, including combustion)  
482 out of all LIs. In Utrecht, the C<sub>2</sub>:C<sub>1</sub> ratio for the LIs attributed to NGDNs is  $3.9 \pm 0.8$  %.

### 483 3.3 Quantification of CH<sub>4</sub> plume from larger facilities

484 Table 3 shows the emission rate estimates from the larger facilities in Utrecht and Hamburg. CH<sub>4</sub> plumes from the  
485 WWTP (Figure 6 and in SI, Sect. S.1.6., Table S5) were intercepted numerous times during the city transects, and the error  
486 estimate in Table 3 represents one standard deviation of 5 sets of measurements where each measurement comprises 2-4  
487 transects during three measurement days (12-Feb.-2018, 24-Apr.2018, and 07-Jan.-2019). Figure 7 shows an example of a fit  
488 of a Gaussian plume to the measurements from the Utrecht WWTP. The derived distance to the source was  $215 \pm 90$  m, the  
489 hourly average wind speed was  $3.5 \pm 1.1$  m s<sup>-1</sup> and the wind direction was  $178 \pm 5$  degrees (see SI, Sect. S.1.6, Table S5).

490 The total emission rate of the WWTP in Utrecht was estimated at  $160 \pm 90$  t yr<sup>-1</sup>. The reported errors include stability  
491 classes, wind speed and directions, and effective point source coordinates. Not all transects provided datasets that allowed an  
492 adequate Gaussian fit, these were not included in total estimates from the facilities, e.g. measurements during the visits of the  
493 harbor area in Hamburg were excluded. In Hamburg, plumes from several facilities were also intercepted several times (see  
494 SI, Sect. S.1.6, Table S6). For a Compost and Soil Company in Hamburg we estimate an emission rate of  $70 \pm 50$  t yr<sup>-1</sup>. The  
495 mobile quantifications at the upstream sites in Hamburg from a separator, a tank, and an oil well yield annual CH<sub>4</sub> emission  
496 of  $4.5 \pm 3.7$  t yr<sup>-1</sup>,  $5.2 \pm 3.0$  t yr<sup>-1</sup>, and  $4.8 \pm 4.0$  t yr<sup>-1</sup> respectively.

## 497 4 Discussion

### 498 4.1 Detection and quantification

499 As mentioned above (see Sect. 2.2.2), we used methods similar to the ones introduced by von Fischer et al. (2017)  
500 and updated in Weller et al. (2019) that were used to characterize CH<sub>4</sub> emission from local gas distribution systems in the US.  
501 An important difference is that we did not visit each street twice in the untargeted survey, and the revisits were specifically  
502 targeted at locations where we had found a LI during the first visit. A consequence of the different sampling strategy is that  
503 we do not base our city-level extrapolated emissions estimates on “confirmed” LIs, as done in Weller et al. (2019) but on all  
504 the LIs observed. In our study, 60 % of CH<sub>4</sub> LIs in Utrecht and 46 % of LIs in Hamburg were confirmed. This number may be  
505 biased high, since we preferentially revisited locations that had shown higher LIs, and the percentage of confirmed LIs may  
506 have been lower if we had visited locations with smaller LIs. Von Fischer et al. (2017) reported that LIs in the high emission  
507 rate category have a 74 % chance of detection, which decreased to 63 % for the middle category and 35 % frequency for the  
508 small category. In our study, all LIs within the high emission rate category (n = 1 and n = 2 LIs in Utrecht and Hamburg  
509 respectively) were confirmed in both cities. Overall, the confirmation rates found in Hamburg and Utrecht were similar to the  
510 ones reported in the US cities by von Fischer et al. (2017), suggesting that the results from both driving strategies can be  
511 compared when we take into account an overall confirmation percentage of roughly 50 %.

512 In 13 US cities the “LI density” ranged from 1 LI per 1.6 km driven to 1 LI per  $\approx 320$  km driven (EDF, 2019). This  
513 illustrates that cities within one country can be very different in their NGDN infrastructure. In Utrecht, one LI was observed  
514 every 5.6 km of street covered and in Hamburg every 8.4 km covered. Note that we normalize the number of LIs per km of  
515 road covered, not km of road driven, since the revisits were targeted to confirm LIs, which would bias the statistics if we  
516 normalize by km of road driven. After accounting for the confirmation percentage of 50 %, the LI densities in Utrecht and  
517 Hamburg become 1 LI per 11.2 km covered in Utrecht, and 1 LI per 16.8 km covered in Hamburg. When we take into account  
518 the attributions (fraction fossil/total LIs is 43 % in Utrecht and 31 % in Hamburg), confirmed LIs from the NGDN are found

519 every 26 km in Utrecht and every 54 km in Hamburg. The highest 1 % of the LIs in Utrecht and Hamburg account for  
520 approximately 30 % of emissions, emphasizing the presence of a skewed distribution of emissions. The emissions distribution  
521 is even more skewed for these two European cities than for countrywide US cities, where approximately 25 % of emissions  
522 comes from the highest 5 % of the LIs. Skewed emission distributions appear to be typical for emissions from the oil and gas  
523 supply chain across different scales. For example, a synthesis study reviewing the distribution of upstream emissions from the  
524 US natural gas system shows that in the US 5 % of the leaks are responsible for 50 % of the emissions (Brandt et al., 2016).

## 525 4.2 Attribution

526 Four different approaches were combined in Hamburg for emission source attribution, which allows an evaluation of  
527 their molecular consistency. Figure 5 shows that measurements of the C<sub>2</sub>:C<sub>1</sub>, δD, and δ<sup>13</sup>C provide a very consistent distinction  
528 between fossil and microbial sources of CH<sub>4</sub>. Except for one outlier with a very enriched δ<sup>13</sup>C and δD contents and no C<sub>2</sub>H<sub>6</sub>  
529 signal, all samples that are classified as “microbial” and depleted in δ<sup>13</sup>C and δD signatures contain no measurable C<sub>2</sub>H<sub>6</sub>.  
530 Samples that are characterized as “fossil”, based on δ<sup>13</sup>C and δD signatures, bear a C<sub>2</sub>H<sub>6</sub> concomitant signal. This strengthens  
531 the confidence in source attribution using these tracers. The fossil δ<sup>13</sup>C signature of bag samples from natural gas leaks in  
532 Hamburg (δ<sup>13</sup>C = -41.9 ± 1.0 ‰) is higher than recent reports from the city of Heidelberg, Germany (δ<sup>13</sup>C = -43.3 ± 0.8 ‰  
533 (Hoheisel et al., 2019)). This shows that within one country, δ<sup>13</sup>C from NGDNs can vary from one region to another. These  
534 numbers do not agree within combined errors, but are also not very different. δ<sup>13</sup>C values of CH<sub>4</sub> from the NGDN can vary  
535 regionally and temporally, e.g. due to differences in the mixture of natural gas from various suppliers for different regions in  
536 Germany (DVGW, 2013). In a comprehensive study at global scale, it is also shown that how δ<sup>13</sup>C values of fossil fuel CH<sub>4</sub>  
537 have significant variabilities in different regions within an individual basin (Figure 4 in Sherwood et al. (2017)).

538 In Hamburg both C<sub>2</sub>:C<sub>1</sub> and CH<sub>4</sub>:CO<sub>2</sub> analysis along with δ<sup>13</sup>C and δD signatures suggest that ≈ 50 % to ≈ 80 % of  
539 estimated emissions (≈ 30 % and ≈ 40 % of LIs respectively) originate from NGDNs, whereas CH<sub>4</sub>:CO<sub>2</sub> analysis and the  
540 smaller sample of C<sub>2</sub>:C<sub>1</sub> measurements in Utrecht suggests that the overwhelming fraction (70 - 90 % of emissions; 40 - 70 %  
541 of LIs) originated from NGDNs. We note that although it is widely assumed that microbial CH<sub>4</sub> is not associated with ethane,  
542 some studies have reported microbial production of ethane, so it may not be a unique identifier (Davis and Squires, 1954;  
543 Fukuda et al., 1984; Gollakota and Jayalakshmi, 1983; Formolo, 2010). The online C<sub>2</sub>:C<sub>1</sub> analysis to attribute LIs is fast and  
544 can be used at larger scale, but with the instrument we used we were not able to clearly attribute sources with CH<sub>4</sub>  
545 enhancements of less than 500 ppb. Isotopic analysis by IRMS can attribute sources for smaller LIs (down to 100-200 ppb)  
546 but is clearly more labor intensive, and it would be a considerable effort to take samples from all LIs observed across an urban  
547 area. Overall, C<sub>2</sub>H<sub>6</sub> and CO<sub>2</sub> signals are very useful in eliminating non-fossil LIs in mobile urban measurements and with  
548 improvements in instrumentations, analyzing signals of these two species along with evaluation of CH<sub>4</sub> signals can make  
549 process of detecting pipeline leaks from NGDN more efficient.

550 In Hamburg, most of the LIs were detected in the city center (Figure 1). This means that the LI density is higher than  
551 the average value in the center, but much lower than the average value in the surrounding districts and residential areas. Many  
552 of the LIs in the city center were attributed to combustion and microbial sources, thus they do not originate from leaks in the  
553 NGDN. Many of the microbial LIs encountered in Hamburg are around the Binnenalster lake (see SI, Sect. S.3.3, Figure S15),  
554 which suggests that anaerobic methanogenesis (Stephenson and Stickland, 1933; Thauer, 1998) can cause these microbial  
555 emission in this lake, as seen in other studies focused on emissions from other lakes (e.g., DelSontro et al., 2018; Townsend-  
556 Small et al., 2016). Microbial CH<sub>4</sub> emissions from sewage system (Guisasola et al., 2008) can also be an important source of  
557 in this area, as seen in US urban cities (Fries et al., 2018). Fries et al. (2018) performed direct measurement of CH<sub>4</sub> and nitrous  
558 oxide (N<sub>2</sub>O) from a total of 104 sites, and analyzed δ<sup>13</sup>C and δD signatures of samples from 27 of these locations, and attributed  
559 47 % of these locations to microbial emissions in Cincinnati, Ohio, USA.

### 560 4.3 Comparison to national inventory reports

561 In the national inventory reports, total upscaled emissions from NGDNs are based on sets of emission factors for  
562 different pipeline materials (e.g., grey cast iron, steel, or plastic) at different pressures (e.g.,  $\leq 200$  mbar or  $>200$  mbar). The  
563 reported emission factors are based on IPCC tier 3 approach (Buendia et al., 2019). However, emission estimates do not exist  
564 for individual cities including Utrecht and Hamburg. Also, it is not possible to calculate a robust city-level estimate using the  
565 nationally reported emission factors because there is no publicly available associated activity data, i.e., pipeline materials and  
566 lengths for each material, at the level of individual cities. As a result, a robust direct comparison between nationally reported  
567 emissions and our measurements, akin to a recent study in the United States (Weller et al., 2020), is currently not possible.  
568 The following juxtaposition of our estimates and national inventory downscaling to city-level is therefore provided primarily  
569 as illustration of the data gaps rather than a scientific comparison. In Utrecht, we attributed 70 – 90 % of the mobile  
570 measurement inferred emissions of  $\approx 150$  t yr<sup>-1</sup> to the NGDN, thus 105 – 135 t yr<sup>-1</sup>.

571 The Netherlands National Institute for Public Health and the Environment (RIVM) inventory report derived an  
572 average NGDN emission factor of  $\approx 110$  kg km<sup>-1</sup> yr<sup>-1</sup> using 65 leak measurements from different pipeline materials and  
573 pressures in 2013. This weighted average ranged from a maximum of 230 kg km<sup>-1</sup> yr<sup>-1</sup> for grey cast iron pipelines to a minimum  
574 of 40 kg km<sup>-1</sup> yr<sup>-1</sup> for pipelines of other materials with overpressures  $\leq 200$  mbar (for details, see P. 130 in Peek et al. (2019)).  
575 This results in an average CH<sub>4</sub> emissions of  $\approx 70$  t yr<sup>-1</sup> (min = 30 t yr<sup>-1</sup> and max = 150 t yr<sup>-1</sup>) for the study area of Utrecht,  
576 assuming  $\approx 650$  km of pipelines inside the ring, and further assuming that Utrecht's NGDN is representative of the national  
577 reported average (see qualifiers above). The average emissions for the Utrecht study, based on emissions factors reported for  
578 the Netherlands, is smaller by a factor of 1.5 - 2 compared to the emissions derived here. The variability factor of 5, from the  
579 reported emission (resulting from the variability in pipeline materials) highlights the need for city-level specific activity  
580 data for a robust comparison. In Hamburg, 50 – 80 % of the upscaled emissions of 440 t yr<sup>-1</sup> (220 – 350 t yr<sup>-1</sup>), can be attributed  
581 to the emission from NGDN. The national inventory from the Federal Environment Agency (UBA) in Germany, reports an  
582 average CH<sub>4</sub> emission factor for NGDN from low pressure pipelines as  $\approx 290$  kg km<sup>-1</sup> yr<sup>-1</sup> (max = 445 kg km<sup>-1</sup> yr<sup>-1</sup> (grey cast  
583 iron) and min = 51 kg km<sup>-1</sup> yr<sup>-1</sup> (plastic)) based on measurements from the 1990s (Table 169 in Federal Environment Agency  
584 (2019)). Assuming  $\approx 3000$  km of pipelines in the targeted region, and further assuming that Hamburg's NGDN is representative  
585 of the national reported average (see qualifiers above), results in an estimated NGDN CH<sub>4</sub> emissions average of  $\approx 870$  t yr<sup>-1</sup>  
586 (min = 155 t yr<sup>-1</sup> and max = 1350 t yr<sup>-1</sup>). While this study's estimate (220 – 350 t yr<sup>-1</sup>) falls in the lower end of this range, the  
587 reported emissions variability factor of 9 (resulting from the variability in pipeline materials) highlights again the need for  
588 city-level specific activity data for a robust comparison. To put the national inventory comparison into perspective, it should  
589 be noted that GasNetz Hamburg detected and fixed leaks at 20 % of the fossil LIs in this study, which accounted for 50 % of  
590 emissions. In Utrecht and Hamburg, the natural gas consumption in our target area were retrieved through communications  
591 with LDCs. In the Utrecht and Hamburg study areas, natural gas consumption is 0.16 bcm yr<sup>-1</sup> (STEDIN, personal  
592 communication) and 0.75 bcm yr<sup>-1</sup> (GasNetz Hamburg, personal communication) respectively. The estimated emissions from  
593 NGDNs in our study is between 0.10 – 0.12 % in Utrecht and between 0.04 – 0.07 % in Hamburg of total the annual natural  
594 gas consumptions in the same area. In the US, where the majority of natural gas consumption is from residential and  
595 commercial sectors, Weller et al. (2020) reported emissions of 0.69 Tg year<sup>-1</sup> (0.25 - 1.23 with 95 % confidence interval), with  
596 a sum of  $\approx 170$  Tg year<sup>-1</sup> (U.S. EIA, 2019), showing 0.4 % (0.15 % - 0.7 %) loss from NGDNs. The US NGDNs loss is about  
597 four times larger than our reported loss in Utrecht, and is about ten times larger than the loss for Hamburg. Considering the  
598 population of Utrecht ( $\approx 0.28$  million) and Hamburg ( $\approx 1.45$  million), the natural gas consumption densities in these study  
599 areas are  $\approx 570$  m<sup>3</sup> capita<sup>-1</sup> yr<sup>-1</sup> and  $\approx 520$  m<sup>3</sup> capita<sup>-1</sup> yr<sup>-1</sup>, where in the US (population  $\approx 330$  million (US Census Bureau,  
600 2020)) the density is about  $\approx 730$  m<sup>3</sup> capita<sup>-1</sup> yr<sup>-1</sup> (see SI, Sect. S.3.2, Figure S14). This shows that annual natural gas  
601 consumption per capita in the US is about 30 % and 40 % higher than in Utrecht and Hamburg respectively. The emission per

602 km of pipeline in Utrecht is between  $0.45 - 0.5 \text{ L min}^{-1} \text{ km}^{-1}$  and in Hamburg is between  $0.2 - 0.32 \text{ L min}^{-1} \text{ km}^{-1}$ . In the US,  
603 based on 2,086,000 km km of local NGDN pipeline (Weller et al., 2020), this emission factor will be between  $0.32 - 1.57 \text{ L}$   
604  $\text{min}^{-1} \text{ km}^{-1}$ . This shows higher emissions per km pipeline in the countrywide studies of US compared to just two European  
605 cities of Utrecht and Hamburg (see qualifiers above). This can be partly explained by pipeline material, maintenance protocols,  
606 and higher use of natural gas consumption in the US. However, the substantial variability in emission rates across US cities,  
607 as wells as the annual variability of gas consumption over the year, again restricts a direct comparison of two cities with a  
608 national average measured over multiple years.

609 Normalized LIs emissions per capita in Utrecht ( $0.54 \pm 0.15 \text{ kg yr}^{-1} \text{ capita}^{-1}$ ) are almost double the emission factor in  
610 Hamburg ( $0.31 \pm 0.04 \text{ kg yr}^{-1} \text{ capita}^{-1}$ ). This metric may be useful to compare cities, assuming that the emission quantification  
611 method is equally effective for different cities.  $\text{CH}_4$  emissions can vary among different cities, depending on the age,  
612 management and material of NGDNs, and/or the management of local sewer systems. In our study, we only surveyed two  
613 cities, and the above number may not be adequate for extrapolation to the country scale (McKain et al., 2015).

#### 614 4.4 Interaction with utilities

615 After the city surveys, locations with the highest emissions (high and medium categories) were shared with STEDIN  
616 Utrecht and all LI locations were reported to GasNetz Hamburg. The utilities repair teams were sent to check whether LIs  
617 could be detected as leaks from NGDN and fixed. The LDCs follow leak detection procedures based on country regulations  
618 (e.g., for GasNetz Hamburg in SI, Sect. S.4.1, Table S11). GasNetz Hamburg also co-located the coordinates of the detected  
619 reported LIs with the NGDN and prioritized repairs based on safety regulations mentioned in Table S12 (see SI, Sect. S.4.1).  
620 This interaction with the LDCs resulted in fixing major NGDN leaks in both cities. In Utrecht the only spot in the high emission  
621 category was reported to STEDIN, but the pipelines on this street had been replaced, which most likely fixed the leak, as it  
622 was not found later by the gas company nor in our later survey with the  $\text{CH}_4 - \text{C}_2\text{H}_6$  analyzer. In Utrecht, half of the LIs in the  
623 medium category were found and repaired.

624 A routine leak survey (detection and repair) had been performed by GasNetz Hamburg between 1-5 months before  
625 the campaign, for the different regions (see SI, Sect. S.4.1., Table S11). The timing of any routine detection and repair likely  
626 influences the absolute number of LIs measured during independent mobile measurements, and the survey by GasNetz  
627 Hamburg thus likely has influenced the absolute number of LIs measured in our campaign. We then reported the LI  
628 latitude/longitude coordinates to GasNetz Hamburg about 4 months after our campaign. Additionally, we provided map images  
629 of the LIs immediately after the campaign. The comparison of the number of reported LIs (and emission rates) during our  
630 campaign with those identified by GasNetz Hamburg post-campaign assumes that the leaks continued to emit gas until they  
631 were detected and fixed by GasNetz Hamburg (if they were detected).

632 Depending on how close the gas leaks are located to a building, the LDCs prioritize the leaks into four classes from  
633 the highest to lowest priority: A1, A2, B, and C (see SI, Sect. S.4.1, Table S12). In Hamburg, both LIs in the high category  
634 were identified as A1 gas leaks and fixed by GasNetz Hamburg immediately. Most of the Hamburg LIs that were detected and  
635 identified as fossil are in close proximity to the natural gas distribution pipelines (see SI, Sect. S.4.2, Table S13). Investigation  
636 of the pipeline material shows that most of NGDN emissions are due to leaks from steel pipelines (see SI, Sect. S.4.2, Table  
637 S14), which are more prone to leakage because of pipeline corrosion (Zhao et al., 2018). Nevertheless, only 7 of the 30 LIs  
638 (23 %) that were positively attributed to fossil  $\text{CH}_4$  were detected and fixed by the LDC. If we assume that the fraction fossil  
639 / total LIs determined in Hamburg ( $\approx 35 \%$ ) is representative for the entire population of LIs encountered (thus also for the  
640 ones that were not attributable), about 50 of the 145 LIs are likely due to fossil  $\text{CH}_4$ . The LDC found and fixed leaks at 10 of  
641 these locations ( $\approx 20 \%$ ). A recent revisit (January 2020) to these locations confirmed that no LIs were detected at 9 out of  
642 these 10 locations. For the 10<sup>th</sup> location a smaller LI was detected in close proximity, and GasNetz Hamburg confirmed that



643 this was a leak from a steel pipeline. The whole pipeline system on this street dates back to the 1930s and is targeted for  
644 replacement in the near future.

645 In summary, about 20 % of the LIs including the two largest LIs that were attributed to a fossil source were identified  
646 as NGDN gas leaks (see SI, Sect. S.4.2, Figure S18), and were repaired by GasNetz Hamburg, but these accounted for about  
647 50 % of fossil CH<sub>4</sub> emissions of Hamburg, similar to what was observed in the US studies (Weller et al., 2018). Possibly,  
648 smaller leakages that can be detected with the high sensitivity instruments used in the mobile surveys cannot be detected with  
649 the less sensitive equipment of LDCs. Another possible explanation for the fact that the LDC did not detect more leaks may  
650 be that reported LI locations do not always coincide with the actual leak locations, although Weller et al. (2018) reported that  
651 the median distance of actual leak locations to the reported ones was 19 m. Combined measurements with GasNetz Hamburg  
652 are planned to investigate why the majority of the smaller LIs reported in mobile surveys is not detected in the regular surveys  
653 of the LDC.

654 The average C<sub>2</sub>:C<sub>1</sub> ratio for LIs with a significant C<sub>2</sub>H<sub>6</sub> signals across Hamburg was  $5.6 \pm 3.9$  %. For the spots where  
655 the LDC found and fixed leaks this ratio was  $3.9 \pm 2.6$  %. Thus, some of the locations where CH<sub>4</sub> enhancements were found  
656 were influenced by sources with an even higher C<sub>2</sub>:C<sub>1</sub> ratio than the gas in the NGDN. One confirmed example is the very  
657 high ratio found in exhaust from a vehicle as shown in Figure S12 (see SI, Sect. S.2.6). The abnormal operation of this vehicle  
658 is confirmed by the very high CH<sub>4</sub>:CO<sub>2</sub> ratio of 5.5 ppb:ppm (SI, section S2). This is more than 20 times higher than CH<sub>4</sub>:CO<sub>2</sub>  
659 ratios of  $0.2 \pm 0.1$  ppb:ppm observed during passages through the Elbe tunnel, a ratio that agrees with previous studies (SI,  
660 section S2).

661 Repairing gas leaks in a city has several benefits for safety (preventing explosions), sustainability (minimizing GHG  
662 emissions) and economics. Gas that is not lost via leaks can be sold for profit, but gas leak detection and repair is expensive  
663 and is usually associated with interruptions of the infrastructure (breaking up pavements and roads). Also, as reported above,  
664 and in agreement with the studies in US cities, for small LIs the underlying leaks are often not found by the LDCs, possibly  
665 because their equipment is less sensitive and aimed for finding leak rates that are potentially dangerous.

666 Our measurements in Hamburg demonstrate that in particular smaller LIs may originate from biogenic sources, e.g.  
667 the sewage system, and not necessarily from leaks in the NGDN. In this respect, attribution of LIs prior to reporting to the  
668 LDCs may be beneficial to facilitate effective repair. Figure S19 (see SI, Sect. S.5) illustrates how the individual measurement  
669 components can be efficiently combined in a city leak survey program.

#### 670 4.5 Large facilities

671 The WWTP in Utrecht emits  $160 \pm 90$  t yr<sup>-1</sup>, which is similar to the total detected emissions ( $150$  t yr<sup>-1</sup>) inside the  
672 study area of Utrecht. The emissions reported for this facility from 2010 until 2017 are  $130 \pm 50$  t yr<sup>-1</sup> (Rijksoverheid, 2019),  
673 in good agreement with our measurements. CH<sub>4</sub> emission from a single well in Hamburg was estimated at  $4.4 \pm 3.5$  t yr<sup>-1</sup>,  
674 which is in the range of median emissions of  $2.3$  t yr<sup>-1</sup> reported for gas production wells in Groningen, NL (Yacovitch et al.,  
675 2018), and average emissions of all US oil and gas production wells  $7.9 \pm 1.8$  t yr<sup>-1</sup> (Alvarez et al., 2018). In Hamburg, the  
676 emissions from a Compost and Soil Company amount to about 10 % of the total emissions in the city target region, whereas a  
677 wellhead, a storage tank and a waste-oil separator contribute only about 1 % each. This shows that individual facilities can  
678 contribute significantly to the total emissions of a city. The contribution of each source is dependent on infrastructure, urban  
679 planning and other conditions in the city (e.g. age and material of pipeline, maintenance programs, waste management, sewer  
680 system conditions, etc.), which may change the source mix from one city to another. For example, in Utrecht the WWTP is  
681 located within our domain of study. The wastewater treatment in Hamburg most likely causes CH<sub>4</sub> emissions elsewhere.  
682 Therefore, facility-scale CH<sub>4</sub> emissions should be reported on a more aggregated provincial or national level. For emissions  
683 from the NGDN, the urban scale is highly relevant, as the emission can only be mitigated at this scale.

## 684 5 Conclusions

685 Mobile measurements provide a fast and accurate technique for observing and identifying even relatively small CH<sub>4</sub>  
686 enhancements (i.e., tens of ppb) across cities and are useful for detecting potential gas leaks. During our intensive measurement  
687 campaigns, 81 LIs were observed in Utrecht (corresponding to emissions of  $\approx 110$  t CH<sub>4</sub> yr<sup>-1</sup>) and 145 LIs ( $\approx 180$  t CH<sub>4</sub> yr<sup>-1</sup>) in  
688 Hamburg. These estimates, based on the streets covered, were then up-scaled to the total study area, using the road network  
689 map as a proxy for the length of the pipeline network which then yielded total emissions of 150 t yr<sup>-1</sup> and 440 t yr<sup>-1</sup> across the  
690 study area of Utrecht and Hamburg respectively. The isotopic signature of CH<sub>4</sub> in air samples and continuous mobile  
691 measurement of CO<sub>2</sub> and C<sub>2</sub>H<sub>6</sub> mole fraction show that not all the LIs observed across the two cities have fossil origin. In  
692 Utrecht, C<sub>2</sub>:C<sub>1</sub> and CH<sub>4</sub>:CO<sub>2</sub> analyses show that 70 -90 % of emissions were fossil. In Hamburg, C<sub>2</sub>:C<sub>1</sub>, CH<sub>4</sub>:CO<sub>2</sub>, and  $\delta^{13}\text{C}$ -  
693  $\delta\text{D}$  analyses suggests that 50 - 80 % of emissions originate from natural gas pipelines. For the locations where samples for  
694 isotope analysis were collected, 80 % of emissions were identified as fossil. A large fraction of emissions in both cities  
695 originated from few high emitting locations. The LDC in Hamburg (GasNetz Hamburg) detected and fixed leaks at 20 % of  
696 the locations that likely due to fossil sources, but these accounted for 50 % of emissions. Large LIs were generally confirmed  
697 as gas leaks from steel pipelines. The C<sub>2</sub>:C<sub>1</sub> ratio at the locations where gas leaks were fixed by GasNetz Hamburg was  $3.9 \pm$   
698 2.6 %. The mobile measurement technique is less labor and time intensive than conventional methods and can provide  
699 extensive coverage across a city in a short period. Based on our experience for the Netherlands and Germany a protocol could  
700 be developed that aids LDCs in guiding their leak detection and repair teams. The use of emission categories and source  
701 attribution can help target repair activities to the locations of large fossil emissions. Emission quantification from large  
702 facilities shows that these emissions may be equivalent to total CH<sub>4</sub> emissions from NGDN leaks in urban environments. In  
703 order to analyze discrepancies between spatial explicit measurement-based estimates as presented here with reported annual  
704 average national emissions by sectors a coordinated effort with national agencies is necessary to address the lack of publicly  
705 available activity data (e.g., pipe material) disaggregated from the national-level (e.g., at the city-level).

706 **Code availability:** A MATLAB® code to analyze urban surveys is available on GitHub from Maazallahi et al. (2020a).

707 **Data availability:** The data including in-situ measurements, GPS data, and boundary of study areas are available on the  
708 Integrated Carbon Observation System (ICOS) portal from Maazallahi et al. (2020b).

709 **Video supplement:** A virtual tour of the measurements is available on the Leibniz Information Centre for Science and  
710 Technology and University Library (TIB) portal from Maazallahi et al. (2020c).

### 711 Author contributions

712 H. M. performed the mobile measurements, wrote the MATLAB® code, analyzed the data, and together with T. R.  
713 drafted the manuscript. J. M. F. and M. M. contributed with air sampling and isotope analysis. D. Z. -A. and S. S. contributed  
714 to the scientific interpretation and comparison between European and US cities. Z. D. W. and J. C. v. F. facilitated comparison  
715 to US cities and contributed to the statistical analysis. H. D. v. d. G. and T. R. provided instruments, equipment, and supervised  
716 the measurements and data analysis. T. R. developed the research idea and coordinated the city campaigns. All authors  
717 contributed to the interpretation of the results and the improvement of the manuscript.

718 **Competing interests:** The authors declare that they have no conflict of interest.

719  
720  
721

## 722 Acknowledgements

723 This work was supported by the Climate and Clean Air Coalition (CCAC) Oil and Gas Methane Science Studies  
724 (MMS) hosted by the United Nations Environment Programme. Funding was provided by the Environmental Defense Fund,  
725 Oil and Gas Climate Initiative, European Commission, and CCAC. This project received further support from the H2020 Marie  
726 Skłodowska-Curie project Methane goes Mobile – Measurements and Modelling (MEMO<sup>2</sup>; <https://h2020-memo2.eu/>), grant  
727 number 722479. Dr. Daniel Zavala-Araiza and Dr. Stefan Schwietzke were funded by the Robertson Foundation. We thank  
728 Dr. Rebecca Fisher who supervised RHUL contribution to the isotopic analysis of Hamburg campaign. Special thanks to Prof.  
729 Stefan Bühler from the Meteorological Institute of Hamburg University and Dr. Stefan Kinne from the Max Planck Institute  
730 for Meteorology for hosting our team during the Hamburg city measurement surveys. We would like to extend our appreciation  
731 to the anonymous referees for the insightful comments which led to improvements of the manuscript. We appreciate continuous  
732 efforts from executive and management boards of GasNetz Hamburg, Dr. Luise Westphal, Michael Dammann, Dr. Ralf Luy,  
733 and Christian Feickert who facilitated productive communications, provided information on the gas infrastructure in Hamburg  
734 and organized leaks repairs with their teams in study area of Hamburg. We also thank asset manager of STEDIN Utrecht,  
735 Ricardo Verhoeve who provided information and planned leaks repairs by STEDIN in Utrecht. We thank Charlotte Große  
736 from DBI Gas and Environmental Technologies GmbH Leipzig (DBI GUT Leipzig) who helped with clarifying information  
737 on reported emission factors provided in national inventory reports. We thank the former MSc students of Utrecht University,  
738 Laurens Stoop and Tim van den Akker who helped with the measurements in Utrecht study area.

739  
740  
741  
742  
743  
744  
745  
746  
747  
748  
749  
750  
751  
752  
753  
754  
755  
756  
757  
758  
759  
760  
761  
762  
763  
764  
765  
766  
767  
768  
769  
770  
771  
772  
773  
774  
775

## 776 References

- 777 ACM: Authority for Consumers and Markets in the Netherlands, Low NOx Burgners (LNBs) gas code, [online] Available  
 778 from: <https://wetten.overheid.nl/BWBR0037935/2018-05-26>, 2018.
- 779 Allen, D. T., Torres, V. M., Thomas, J., Sullivan, D. W., Harrison, M., Hendler, A., Herndon, S. C., Kolb, C. E., Fraser, M.  
 780 P., Hill, A. D., Lamb, B. K., Miskimins, J., Sawyer, R. F. and Seinfeld, J. H.: Measurements of methane emissions at  
 781 natural gas production sites in the United States, *Proc. Natl. Acad. Sci.*, 110(44), 17768–17773,  
 782 doi:10.1073/pnas.1304880110, 2013.
- 783 Alvarez, R. A., Zavala-Araiza, D., Lyon, D. R., Allen, D. T., Barkley, Z. R., Brandt, A. R., Davis, K. J., Herndon, S. C., Jacob,  
 784 D. J., Karion, A., Kort, E. A., Lamb, B. K., Lauvaux, T., Maasackers, J. D., Marchese, A. J., Omara, M., Pacala, S.  
 785 W., Peischl, J., Robinson, A. L., Shepson, P. B., Sweeney, C., Townsend-Small, A., Wofsy, S. C. and Hamburg, S.  
 786 P.: Assessment of methane emissions from the U.S. oil and gas supply chain., *Science*, 361(6398), 186–188,  
 787 doi:10.1126/science.aar7204, 2018.
- 788 Brandt, A. R., Heath, G. A. and Cooley, D.: Methane Leaks from Natural Gas Systems Follow Extreme Distributions, *Environ.*  
 789 *Sci. Technol.*, 50(22), 12512–12520, doi:10.1021/acs.est.6b04303, 2016.
- 790 Brantley, H. L., Hagler, G. S. W., Kimbrough, E. S., Williams, R. W., Mukerjee, S. and Neas, L. M.: Mobile air monitoring  
 791 data-processing strategies and effects on spatial air pollution trends, *Atmos. Meas. Tech.*, 7(7), 2169–2183,  
 792 doi:10.5194/amt-7-2169-2014, 2014.
- 793 Brass, M. and Röckmann, T.: Continuous-flow isotope ratio mass spectrometry method for carbon and hydrogen isotope  
 794 measurements on atmospheric methane, *Atmos. Meas. Tech.*, 3(6), 1707–1721, doi:10.5194/amt-3-1707-2010, 2010.
- 795 Bright, E. A., Coleman, P. R. and Dobson, J. E.: LandScan : A Global Population database for estimating populations at risk,  
 796 [online] Available from: <https://www.semanticscholar.org/paper/LandScan-%3A-A-Global-Population-database-for-at-risk-Bright-Coleman/17e6076b6761788684434d1e14e85e8877fc0146> (Accessed 23 September 2019), 2000.
- 798 Brümmer, B., Lange, I. and Konow, H.: Atmospheric boundary layer measurements at the 280 m high Hamburg weather mast  
 799 1995-2011: mean annual and diurnal cycles, *Meteorol. Zeitschrift*, 21(4), 319–335, doi:10.1127/0941-  
 800 2948/2012/0338, 2012.
- 801 Buendia, E. C., Guendehou, S., Limmeechokchai, B., Pipatti, R., Rojas, Y., Sturgiss, R., Tanabe, K., Wirth, T., Romano, D.,  
 802 Witi, J., Garg, A., Weitz, M. M., Cai, B., Ottinger, D. A., Dong, H., MacDonald, J. D., Ogle, S. M., Rocha, M. T.,  
 803 Sanchez, M. J. S., Bartram, D. M. and Towprayoon, S.: 2019 refinement to the 2006 IPCC guidelines for national  
 804 greenhouse gas inventories. [online] Available from: <https://www.ipcc.ch/report/2019-refinement-to-the-2006-ipcc-guidelines-for-national-greenhouse-gas-inventories/>, 2019.
- 806 Bukowiecki, N., Dommen, J., Prévôt, A. S. H., Richter, R., Weingartner, E. and Baltensperger, U.: A mobile pollutant  
 807 measurement laboratory - Measuring gas phase and aerosol ambient concentrations with high spatial and temporal  
 808 resolution, *Atmos. Environ.*, 36(36–37), 5569–5579, doi:10.1016/S1352-2310(02)00694-5, 2002.
- 809 Caulton, D. R., Li, Q., Bou-Zeid, E., Fitts, J. P., Golston, L. M., Pan, D., Lu, J., Lane, H. M., Buchholz, B., Guo, X., McSpirt,  
 810 J., Wendt, L. and Zondlo, M. A.: Quantifying uncertainties from mobile-laboratory-derived emissions of well pads  
 811 using inverse Gaussian methods, *Atmos. Chem. Phys.*, 18(20), 15145–15168, doi:10.5194/acp-18-15145-2018, 2018.
- 812 Chamberlain, S. D., Ingrassia, A. R. and Sparks, J. P.: Sourcing methane and carbon dioxide emissions from a small city:  
 813 Influence of natural gas leakage and combustion, *Environ. Pollut.*, 218, 102–110,  
 814 doi:10.1016/j.envpol.2016.08.036, 2016.
- 815 Chen, J., Dietrich, F., Maazallahi, H., Forstmaier, A., Winkler, D., Hofmann, M. E. G., Denier van der Gon, H. and Röckmann,  
 816 T.: Methane emissions from the Munich Oktoberfest, *Atmos. Chem. Phys.*, 20(6), 3683–3696, doi:10.5194/acp-20-  
 817 3683-2020, 2020.
- 818 Curran, S. J., Wagner, R. M., Graves, R. L., Keller, M. and Green, J. B.: Well-to-wheel analysis of direct and indirect use of  
 819 natural gas in passenger vehicles, *Energy*, 75, 194–203, doi:10.1016/j.energy.2014.07.035, 2014.
- 820 Davis, J. B. and Squires, R. M.: Detection of Microbially Produced Gaseous Hydrocarbons Other than Methane., *Science*,  
 821 119(3090), 381–2, doi:10.1126/science.119.3090.381, 1954.
- 822 DelSontro, T., Beaulieu, J. J. and Downing, J. A.: Greenhouse gas emissions from lakes and impoundments: Upscaling in the  
 823 face of global change, *Limnol. Oceanogr. Lett.*, 3(3), 64–75, doi:10.1002/lol2.10073, 2018.
- 824 DVGW: Technische Regel – ArbeitsblattDVGW G 260 (A), Bonn. [online] Available from:  
 825 [https://shop.wvgw.de/var/assets/leseprobe/508866\\_lp\\_G\\_260.pdf](https://shop.wvgw.de/var/assets/leseprobe/508866_lp_G_260.pdf), 2013.
- 826 E. K. Nam, T. E. Jensen, A. and Wallington, T. J.: Methane Emissions from Vehicles, *Environ. Sci. Technol.*,  
 827 doi:10.1021/ES034837G, 2004.
- 828 EDF: Local leaks impact global climate, [online] Available from: <https://www.edf.org/climate/methanemaps> (Accessed 5  
 829 November 2019), 2019.
- 830 Efron, B.: Bootstrap Methods: Another Look at the Jackknife, *Ann. Stat.*, 7(1), 1–26, doi:10.1214/aos/1176344552, 1979.
- 831 Efron, B.: The Jackknife, the Bootstrap and Other Resampling Plans, Society for Industrial and Applied Mathematics., 1982.
- 832 Efron, B. and Tibshirani, R. J.: An Introduction to the Bootstrap, Chapman & Hall, London., 1993.
- 833 EPA: User’s guide for the industrial source guide complex (ISC3) dispersion models, volume II - Description of model  
 834 algorithms., 1995.
- 835 Etheridge, D. M., Steele, L. P., Francey, R. J. and Langenfeld, R. L.: Atmospheric methane between 1000 A.D. and present:  
 836 Evidence of anthropogenic emissions and climatic variability, *J. Geophys. Res.*, 103, 979–993, doi:10.1029/1988JD-00923, 1998.

838 Etminan, M., Myhre, G., Highwood, E. J. and Shine, K. P.: Radiative forcing of carbon dioxide, methane, and nitrous oxide:  
839 A significant revision of the methane radiative forcing, *Geophys. Res. Lett.*, 43(24), 12,614–12,623,  
840 doi:10.1002/2016GL071930@10.1002/(ISSN)1944-8007.2016GRLEDHIGH, 2016.

841 Federal Environment Agency: National Inventory Report for the German Greenhouse Gas Inventory 1990 – 2017. [online]  
842 Available from: <https://unfccc.int/documents/194930>, 2019.

843 von Fischer, J. C., Cooley, D., Chamberlain, S., Gaylord, A., Griebenow, C. J., Hamburg, S. P., Salo, J., Schumacher, R.,  
844 Theobald, D. and Ham, J.: Rapid, Vehicle-Based Identification of Location and Magnitude of Urban Natural Gas  
845 Pipeline Leaks, *Environ. Sci. Technol.*, 51(7), 4091–4099, doi:10.1021/acs.est.6b06095, 2017.

846 Fisher, R., Lowry, D., Wilkin, O., Sriskantharajah, S. and Nisbet, E. G.: High-precision, automated stable isotope analysis of  
847 atmospheric methane and carbon dioxide using continuous-flow isotope-ratio mass spectrometry, *Rapid Commun.*  
848 *Mass Spectrom.*, 20(2), 200–208, 2006.

849 Fisher, R. E., Sriskantharajah, S., Lowry, D., Lanoisellé, M., Fowler, C. M. R., James, R. H., Hermansen, O., Lund Myhre, C.,  
850 Stohl, A., Greinert, J., Nisbet-Jones, P. B. R., Mienert, J. and Nisbet, E. G.: Arctic methane sources: Isotopic evidence  
851 for atmospheric inputs, *Geophys. Res. Lett.*, 38(21), n/a-n/a, doi:10.1029/2011GL049319, 2011.

852 Formolo, M.: The Microbial Production of Methane and Other Volatile Hydrocarbons, in *Handbook of Hydrocarbon and Lipid*  
853 *Microbiology*, pp. 113–126, Springer Berlin Heidelberg, 2010.

854 France, J. L., Cain, M., Fisher, R. E., Lowry, D., Allen, G., O’Shea, S. J., Illingworth, S., Pyle, J., Warwick, N., Jones, B. T.,  
855 Gallagher, M. W., Bower, K., Le Breton, M., Percival, C., Muller, J., Welpott, A., Bauguitte, S., George, C., Hayman,  
856 G. D., Manning, A. J., Myhre, C. L., Lanoisellé, M. and Nisbet, E. G.: Measurements of  $\delta^{13}\text{C}$  in  $\text{CH}_4$  and using  
857 particle dispersion modeling to characterize sources of Arctic methane within an air mass, *J. Geophys. Res. Atmos.*,  
858 121(23), 14,257–14,270, doi:10.1002/2016JD026006, 2016.

859 Fries, A. E., Schifman, L. A., Shuster, W. D. and Townsend-Small, A.: Street-level emissions of methane and nitrous oxide  
860 from the wastewater collection system in Cincinnati, Ohio, *Environ. Pollut.*, 236, 247–256,  
861 doi:10.1016/j.envpol.2018.01.076, 2018.

862 Fukuda, H., Fujii, T. and Ogawa, T.: Microbial Production of  $\text{C}_2$ -Hydrocarbons, Ethane, Ethylene and Acetylene, *Agric. Biol.*  
863 *Chem.*, 48(5), 1363–1365, doi:10.1080/00021369.1984.10866323, 1984.

864 Gallagher, M. E., Down, A., Ackley, R. C., Zhao, K., Phillips, N. and Jackson, R. B.: Natural Gas Pipeline Replacement  
865 Programs Reduce Methane Leaks and Improve Consumer Safety, *Environ. Sci. Technol. Lett.*, 2(10), 286–291,  
866 doi:10.1021/acs.estlett.5b00213, 2015.

867 Gioli, B., Toscano, P., Lugato, E., Matese, A., Miglietta, F., Zaldei, A. and Vaccari, F. P.: Methane and carbon dioxide fluxes  
868 and source partitioning in urban areas: The case study of Florence, Italy, *Environ. Pollut.*, 164, 125–131,  
869 doi:10.1016/j.envpol.2012.01.019, 2012.

870 Gollakota, K. G. and Jayalakshmi, B.: Biogas (natural gas?) production by anaerobic digestion of oil cake by a mixed culture  
871 isolated from cow dung, *Biochem. Biophys. Res. Commun.*, 110(1), 32–35, doi:10.1016/0006-291X(83)91255-X,  
872 1983.

873 Guisasola, A., de Haas, D., Keller, J. and Yuan, Z.: Methane formation in sewer systems, *Water Res.*, 42(6–7), 1421–1430,  
874 doi:10.1016/j.watres.2007.10.014, 2008.

875 Heilig, G. K.: The greenhouse gas methane ( $\text{CH}_4$ ): Sources and sinks, the impact of population growth, possible interventions,  
876 *Popul. Environ.*, 16(2), 109–137, doi:10.1007/BF02208779, 1994.

877 Helfter, C., Tremper, A. H., Halios, C. H., Kotthaus, S., Bjorkegren, A., Sue, C., Grimmond, B., Barlow, J. F. and Nemitz, E.:  
878 Spatial and temporal variability of urban fluxes of methane, carbon monoxide and carbon dioxide above London,  
879 UK, *Atmos. Chem. Phys.*, 16, 10543–10557, doi:10.5194/acp-16-10543-2016, 2016.

880 Helmig, D., Rossabi, S., Hueber, J., Tans, P., Montzka, S. A., Masarie, K., Thoning, K., Plass-Duelmer, C., Claude, A.,  
881 Carpenter, L. J., Lewis, A. C., Punjabi, S., Reimann, S., Vollmer, M. K., Steinbrecher, R., Hannigan, J. W., Emmons,  
882 L. K., Mahieu, E., Franco, B., Smale, D. and Pozzer, A.: Reversal of global atmospheric ethane and propane trends  
883 largely due to US oil and natural gas production, *Nat. Geosci.*, 9(7), 490–495, doi:10.1038/ngeo2721, 2016.

884 Hendrick, M. F., Ackley, R., Sanaie-Movahed, B., Tang, X. and Phillips, N. G.: Fugitive methane emissions from leak-prone  
885 natural gas distribution infrastructure in urban environments, *Environ. Pollut.*, 213, 710–716,  
886 doi:10.1016/j.envpol.2016.01.094, 2016.

887 Hmiel, B., Petrenko, V. V., Dyonisius, M. N., Buizert, C., Smith, A. M., Place, P. F., Harth, C., Beaudette, R., Hua, Q., Yang,  
888 B., Vimont, I., Michel, S. E., Severinghaus, J. P., Etheridge, D., Bromley, T., Schmitt, J., Faïn, X., Weiss, R. F. and  
889 Dlugokencky, E.: Preindustrial  $14\text{CH}_4$  indicates greater anthropogenic fossil  $\text{CH}_4$  emissions, *Nature*, 578,  
890 doi:10.1038/s41586-020-1991-8, 2020.

891 Hoheisel, A., Yeman, C., Dinger, F., Eckhardt, H. and Schmidt, M.: An improved method for mobile characterisation of  $\delta^{13}\text{C}$   
892  $\text{CH}_4$  source signatures and its application in Germany, *Atmos. Meas. Tech.*, 12(2), 1123–1139, doi:10.5194/amt-12-  
893 1123-2019, 2019.

894 Hopkins, F. M., Kort, E. A., Bush, S. E., Ehleringer, J. R., Lai, C.-T., Blake, D. R. and Randerson, J. T.: Spatial patterns and  
895 source attribution of urban methane in the Los Angeles Basin, *J. Geophys. Res. Atmos.*, 121(5), 2490–2507,  
896 doi:10.1002/2015JD024429, 2016.

897 Hu, N., Liu, S., Gao, Y., Xu, J., Zhang, X., Zhang, Z. and Lee, X.: Large methane emissions from natural gas vehicles in  
898 Chinese cities, *Atmos. Environ.*, 187, 374–380, doi:10.1016/j.atmosenv.2018.06.007, 2018.

899 IPCC: Guidelines for national greenhouse inventories. [online] Available from: [https://www.ipcc-](https://www.ipcc-nggip.iges.or.jp/public/gl/guidelin/ch1ref8.pdf)  
900 [nggip.iges.or.jp/public/gl/guidelin/ch1ref8.pdf](https://www.ipcc-nggip.iges.or.jp/public/gl/guidelin/ch1ref8.pdf), 1996.

- 901 Jackson, R. B., Down, A., Phillips, N. G., Ackley, R. C., Cook, C. W., Plata, D. L. and Zhao, K.: Natural gas pipeline leaks  
902 across Washington, DC, *Environ. Sci. Technol.*, 48(3), 2051–2058, doi:10.1021/es404474x, 2014.
- 903 Karion, A., Sweeney, C., Pétron, G., Frost, G., Michael Hardesty, R., Kofler, J., Miller, B. R., Newberger, T., Wolter, S.,  
904 Banta, R., Brewer, A., Dlugokencky, E., Lang, P., Montzka, S. A., Schnell, R., Tans, P., Trainer, M., Zamora, R. and  
905 Conley, S.: Methane emissions estimate from airborne measurements over a western United States natural gas field,  
906 *Geophys. Res. Lett.*, 40(16), 4393–4397, doi:10.1002/grl.50811, 2013.
- 907 Keeling, C. D.: The concentration and isotopic abundances of atmospheric carbon dioxide in rural areas, *Geochim.*  
908 *Cosmochim. Acta*, 13(4), 322–334, doi:10.1016/0016-7037(58)90033-4, 1958.
- 909 Keeling, C. D.: The concentration and isotopic abundances of carbon dioxide in rural and marine air, *Geochim. Cosmochim.*  
910 *Acta*, 24(3–4), 277–298, doi:10.1016/0016-7037(61)90023-0, 1961.
- 911 Lamb, B. K., Cambaliza, M. O. L., Davis, K. J., Edburg, S. L., Ferrara, T. W., Floerchinger, C., Heimbürger, A. M. F., Herndon,  
912 S., Lauvaux, T., Lavoie, T., Lyon, D. R., Miles, N., Prasad, K. R., Richardson, S., Roscioli, J. R., Salmon, O. E.,  
913 Shepson, P. B., Stirm, B. H. and Whetstone, J.: Direct and Indirect Measurements and Modeling of Methane  
914 Emissions in Indianapolis, Indiana, *Environ. Sci. Technol.*, 50(16), 8910–8917, doi:10.1021/acs.est.6b01198, 2016.
- 915 LBEG: Geoinformation of Lower Saxony and Schleswig-Holstein, [online] Available from: <https://nibis.lbeg.de/cardomap3/>,  
916 2018.
- 917 Lebel, E. D., Lu, H. S., Speizer, S. A., Finnegan, C. J. and Jackson, R. B.: Quantifying Methane Emissions from Natural Gas  
918 Water Heaters, *Environ. Sci. Technol.*, 54(9), 5737–5745, doi:10.1021/acs.est.9b07189, 2020.
- 919 Lowry, D., Fisher, R. E., France, J. L., Coleman, M., Lanoisellé, M., Zazzeri, G., Nisbet, E. G., Shaw, J. T., Allen, G., Pitt, J.  
920 and Ward, R. S.: Environmental baseline monitoring for shale gas development in the UK: Identification and  
921 geochemical characterisation of local source emissions of methane to atmosphere, *Sci. Total Environ.*, 708, 134600,  
922 doi:10.1016/j.scitotenv.2019.134600, 2020.
- 923 Lyon, D. R., Zavala-Araiza, D., Alvarez, R. A., Harriss, R., Palacios, V., Lan, X., Talbot, R., Lavoie, T., Shepson, P.,  
924 Yacovitch, T. I., Herndon, S. C., Marchese, A. J., Zimmerle, D., Robinson, A. L. and Hamburg, S. P.: Constructing  
925 a Spatially Resolved Methane Emission Inventory for the Barnett Shale Region, *Environ. Sci. Technol.*, 49(13), 8147–  
926 8157, doi:10.1021/es506359c, 2015.
- 927 Lyon, D. R., Alvarez, R. A., Zavala-Araiza, D., Brandt, A. R., Jackson, R. B. and Hamburg, S. P.: Aerial Surveys of Elevated  
928 Hydrocarbon Emissions from Oil and Gas Production Sites, *Environ. Sci. Technol.*, 50(9), 4877–4886,  
929 doi:10.1021/acs.est.6b00705, 2016.
- 930 Maazallahi, H., Fernandez, J. M., Menoud, M., Zavala-Araiza, D., Weller, Z. D., Schwietzke, S., von Fischer, J. C., Denier  
931 van der Gon, H., and Röckmann, T.: MATLAB® code for evaluation of Urban Surveys, Zenodo, doi:  
932 10.5281/zenodo.3928972, 2020a.
- 933 Maazallahi, H., Fernandez, J. M., Menoud, M., Zavala-Araiza, D., Weller, Z. D., Schwietzke, S., von Fischer, J. C., Denier  
934 van der Gon, H., and Röckmann, T.: Utrecht and Hamburg city measurements data, ICOS,  
935 <https://doi.org/10.18160/RAJS-KZZQ>, 2020b.
- 936 Maazallahi, H., Fernandez, J. M., Menoud, M., Zavala-Araiza, D., Weller, Z. D., Schwietzke, S., von Fischer, J. C., Denier  
937 van der Gon, H. and Röckmann, T.: Virtual Tour of Urban Surveys in Utrecht, NL, and Hamburg, DE, TIB AV-  
938 Portal, <https://doi.org/10.5446/49902>, 2020c.
- 939 MacFarling Meure, C., Etheridge, D., Trudinger, C., Steele, P., Langenfelds, R., van Ommen, T., Smith, A. and Elkins, J.:  
940 Law Dome CO<sub>2</sub>, CH<sub>4</sub> and N<sub>2</sub>O ice core records extended to 2000 years BP, *Geophys. Res. Lett.*, 33(14), L14810,  
941 doi:10.1029/2006GL026152, 2006.
- 942 McKain, K., Down, A., Raciti, S. M., Budney, J., Hutyrá, L. R., Floerchinger, C., Herndon, S. C., Nehrkorn, T., Zahniser, M.  
943 S., Jackson, R. B., Phillips, N. and Wofsy, S. C.: Methane emissions from natural gas infrastructure and use in the  
944 urban region of Boston, Massachusetts, *Proc. Natl. Acad. Sci.*, 112(7), 1941–1946, doi:10.1073/PNAS.1416261112,  
945 2015.
- 946 Mitchell, A. L., Tkacik, D. S., Roscioli, J. R., Herndon, S. C., Yacovitch, T. I., Martinez, D. M., Vaughn, T. L., Williams, L.  
947 L., Sullivan, M. R., Floerchinger, C., Omara, M., Subramanian, R., Zimmerle, D., Marchese, A. J. and Robinson, A.  
948 L.: Measurements of Methane Emissions from Natural Gas Gathering Facilities and Processing Plants: Measurement  
949 Results, *Environ. Sci. Technol.*, 49(5), 3219–3227, doi:10.1021/es5052809, 2015.
- 950 Myhre, G., Shindell, D., Bréon, F. M., Collins, W., Fuglestedt, J., Huang, J., Koch, D., Lamarque, J. F., Lee, D., Mendoza,  
951 B., Nakajima, T., Robock, A., Stephens, G., Takemura, T. and Zhan, H.: Anthropogenic and Natural Radiative Forc-  
952 ing. In: *Climate Change 2013: The Physical Science Basis. Contribution of Working Group I to the Fifth Assessment*  
953 *Report of the Intergovernmental Panel on Climate Change*, Cambridge, United Kingdom and New York, NY, USA.  
954 [online] Available from: [https://www.ipcc.ch/site/assets/uploads/2018/02/WG1AR5\\_Chapter08\\_FINAL.pdf](https://www.ipcc.ch/site/assets/uploads/2018/02/WG1AR5_Chapter08_FINAL.pdf), 2013.
- 955 Naus, S., Röckmann, T. and Popa, M. E.: The isotopic composition of CO in vehicle exhaust, *Atmos. Environ.*, 177, 132–142,  
956 doi:10.1016/J.ATMOSENV.2018.01.015, 2018.
- 957 Neumann, G. and Halbritter, G.: Sensitivity analysis of the Gaussian plume model, in *Studies in Environmental Science*, vol.  
958 8, pp. 57–62, Elsevier., 1980.
- 959 Noël, S., Weigel, K., Bramstedt, K., Rozanov, A., Weber, M., Bovensmann, H. and Burrows, J. P.: Water vapour and methane  
960 coupling in the stratosphere observed using SCIAMACHY solar occultation measurements, *Atmos. Chem. Phys.*,  
961 18(7), 4463–4476, doi:10.5194/acp-18-4463-2018, 2018.
- 962 O’Shea, S. J., Allen, G., Fleming, Z. L., Bauguitté, S. J.-B., Percival, C. J., Gallagher, M. W., Lee, J., Helfter, C. and Nemitz,  
963 E.: Area fluxes of carbon dioxide, methane, and carbon monoxide derived from airborne measurements around

- 964 Greater London: A case study during summer 2012, *J. Geophys. Res. Atmos.*, 119(8), 4940–4952,  
965 doi:10.1002/2013JD021269, 2014.
- 966 Omara, M., Sullivan, M. R., Li, X., Subramanian, R., Robinson, A. L. and Presto, A. A.: Methane Emissions from  
967 Conventional and Unconventional Natural Gas Production Sites in the Marcellus Shale Basin, *Environ. Sci. Technol.*,  
968 50(4), 2099–2107, doi:10.1021/acs.est.5b05503, 2016.
- 969 Paredes, M. G., Güereca, L. P., Molina, L. T. and Noyola, A.: Methane emissions from anaerobic sludge digesters in Mexico:  
970 On-site determination vs. IPCC Tier 1 method, *Sci. Total Environ.*, 656, 468–474,  
971 doi:10.1016/j.scitotenv.2018.11.373, 2019.
- 972 Peek, C. J., Montfoort, J. A., Dröge, R., Guis, B., Baas, K., Huet, B. van, Hunnik, O. R. van and Berghe, A. C. W. M. van den:  
973 Methodology report on the calculation of emissions to air from the sectors Energy, Industry and Waste, as used by  
974 the Dutch Pollutant Release and Transfer Register., 2019.
- 975 Phillips, N. G., Ackley, R., Crosson, E. R., Down, A., Hutyra, L. R., Brondfield, M., Karr, J. D., Zhao, K. and Jackson, R. B.:  
976 Mapping urban pipeline leaks: Methane leaks across Boston, *Environ. Pollut.*, 173, 1–4,  
977 doi:10.1016/j.envpol.2012.11.003, 2013.
- 978 Popa, M. E., Vollmer, M. K., Jordan, A., Brand, W. A., Pathirana, S. L., Rothe, M. and Röckmann, T.: Vehicle emissions of  
979 greenhouse gases and related tracers from a tunnel study: CO : CO<sub>2</sub>, N<sub>2</sub>O : CO<sub>2</sub>, CH<sub>4</sub> : CO<sub>2</sub>, O<sub>2</sub> : CO<sub>2</sub> ratios, and  
980 the stable isotopes <sup>13</sup>C and <sup>18</sup>O in CO<sub>2</sub> and CO, *Atmos. Chem. Phys.*, 14(4), 2105–2123, doi:10.5194/acp-14-2105-  
981 2014, 2014.
- 982 Prather, M. J., Holmes, C. D. and Hsu, J.: Reactive greenhouse gas scenarios: Systematic exploration of uncertainties and the  
983 role of atmospheric chemistry, *Geophys. Res. Lett.*, 39(9), n/a-n/a, doi:10.1029/2012GL051440, 2012.
- 984 Rijksoverheid: Emissieregistratie. [online] Available from: <http://www.emissieregistratie.nl/erpubliek/erpub/facility.aspx>  
985 (Accessed 9 December 2019), 2019.
- 986 Röckmann, T., Eyer, S., van der Veen, C., Popa, M. E., Tuzson, B., Monteil, G., Houweling, S., Harris, E., Brunner, D.,  
987 Fischer, H., Zazzeri, G., Lowry, D., Nisbet, E. G., Brand, W. A., Necki, J. M., Emmenegger, L. and Mohn, J.: In situ  
988 observations of the isotopic composition of methane at the Cabauw tall tower site, *Atmos. Chem. Phys.*, 16(16),  
989 10469–10487, doi:10.5194/acp-16-10469-2016, 2016.
- 990 Schaum, C., Lensch, D., Bolle, P. Y. and Cornel, P.: Sewage sludge treatment: Evaluation of the energy potential and methane  
991 emissions with cod balancing, *J. Water Reuse Desalin.*, 5(4), 437–445, doi:10.2166/wrd.2015.129, 2015.
- 992 Schmidt, G. A. and Shindell, D. T.: Atmospheric composition, radiative forcing, and climate change as a consequence of a  
993 massive methane release from gas hydrates, *Paleoceanography*, 18(1), n/a-n/a, doi:10.1029/2002PA000757, 2003.
- 994 Schwietzke, S., Sherwood, O. A., Bruhwiler, L. M. P., Miller, J. B., Etiope, G., Dlugokencky, E. J., Michel, S. E., Arling, V.  
995 A., Vaughn, B. H., White, J. W. C. and Tans, P. P.: Upward revision of global fossil fuel methane emissions based  
996 on isotope database, *Nature*, 538(7623), 88–91, doi:10.1038/nature19797, 2016.
- 997 Sherwood, O. A., Schwietzke, S., Arling, V. A. and Etiope, G.: Global Inventory of Gas Geochemistry Data from Fossil Fuel,  
998 Microbial and Burning Sources, version 2017, *Earth Syst. Sci. Data*, 9(2), 639–656, doi:10.5194/essd-9-639-2017,  
999 2017.
- 1000 Sperlich, P., Uitslag, N. A. M., Richter, J. M., Rothe, M., Geilmann, H., van der Veen, C., Röckmann, T., Blunier, T. and  
1001 Brand, W. A.: Development and evaluation of a suite of isotope reference gases for methane in air, *Atmos. Meas.  
1002 Tech.*, 9(8), 3717–3737, doi:10.5194/amt-9-3717-2016, 2016.
- 1003 Stephenson, M. and Stickland, L. H.: Hydrogenase: The bacterial formation of methane by the reduction of one-carbon  
1004 compounds by molecular hydrogen, *Biochem. J.*, 27(5), 1517–1527, doi:10.1042/bj0271517, 1933.
- 1005 Thauer, R. K.: Biochemistry of methanogenesis: a tribute to Marjory Stephenson:1998 Marjory Stephenson Prize Lecture,  
1006 *Microbiology*, 144(9), 2377–2406, doi:10.1099/00221287-144-9-2377, 1998.
- 1007 Tong, L. I., Chang, C. W., Jin, S. E. and Saminathan, R.: Quantifying uncertainty of emission estimates in National Greenhouse  
1008 Gas Inventories using bootstrap confidence intervals, *Atmos. Environ.*, 56, 80–87,  
1009 doi:10.1016/j.atmosenv.2012.03.063, 2012.
- 1010 Townsend-Small, A., Disbennett, D., Fernandez, J. M., Ransohoff, R. W., Mackay, R. and Bourbonniere, R. A.: Quantifying  
1011 emissions of methane derived from anaerobic organic matter respiration and natural gas extraction in Lake Erie,  
1012 *Limnol. Oceanogr.*, 61(S1), S356–S366, doi:10.1002/lno.10273, 2016.
- 1013 Turner, A. J., Frankenberg, C. and Kort, E. A.: Interpreting contemporary trends in atmospheric methane, *Proc. Natl. Acad.  
1014 Sci.*, 116(8), 2805–2813, doi:10.1073/PNAS.1814297116, 2019.
- 1015 Turner, D. B.: Workbook of Atmospheric Dispersion Estimates, U.S. Environmental Protection Agency. [online] Available  
1016 from: <https://nepis.epa.gov/Exe/ZyPDF.cgi/9101GKEZ.PDF?Dockey=9101GKEZ.PDF>, 1969.
- 1017 U.S. EIA: Natural gas consumptions in the United States, [online] Available from:  
1018 <https://www.eia.gov/energyexplained/natural-gas/use-of-natural-gas.php> (Accessed 16 June 2020), 2019.
- 1019 Van Ulden, A. P. and Wieringa, J.: Atmospheric boundary layer research at Cabauw, *Boundary-Layer Meteorol.*, 78(1–2), 39–  
1020 69, doi:10.1007/BF00122486, 1996.
- 1021 Umezawa, T., Brenninkmeijer, C. A. M., Röckmann, T., van der Veen, C., Tyler, S. C., Fujita, R., Morimoto, S., Aoki, S.,  
1022 Sowers, T., Schmitt, J., Bock, M., Beck, J., Fischer, H., Michel, S. E., Vaughn, B. H., Miller, J. B., White, J. W. C.,  
1023 Brailsford, G., Schaefer, H., Sperlich, P., Brand, W. A., Rothe, M., Blunier, T., Lowry, D., Fisher, R. E., Nisbet, E.  
1024 G., Rice, A. L., Bergamaschi, P., Veidt, C. and Levin, I.: Interlaboratory comparison of  $\delta^{13}\text{C}$  and  $\delta\text{D}$  measurements  
1025 of atmospheric CH<sub>4</sub> for combined use of data sets from different laboratories, *Atmos. Meas. Tech.*, 11(2), 1207–  
1026 1231, doi:10.5194/amt-11-1207-2018, 2018.

1027 UNI MISKOLC and ETE: A register of all gas regulations and norms concerning the necessary gas quality for allowing the  
1028 transport in the natural gas grid. [online] Available from: [https://ec.europa.eu/energy/intelligent/projects/sites/iee-projects/files/projects/documents/redubar\\_a\\_register\\_of\\_all\\_gas\\_regulations.pdf](https://ec.europa.eu/energy/intelligent/projects/sites/iee-projects/files/projects/documents/redubar_a_register_of_all_gas_regulations.pdf), 2008.

1030 US Census Bureau: U.S. and World Population Clock, [online] Available from: <https://www.census.gov/popclock/> (Accessed  
1031 20 June 2020), 2020.

1032 Weller, Z., Hamburg, S. P. and von Fischer, J. C.: A national estimate of methane leakage from pipeline mains in natural gas  
1033 local distribution systems, *Environ. Sci. Technol.*, doi:10.1021/acs.est.0c00437, 2020.

1034 Weller, Z. D., Roscioli, J. R., Daube, W. C., Lamb, B. K., Ferrara, T. W., Brewer, P. E. and von Fischer, J. C.: Vehicle-Based  
1035 Methane Surveys for Finding Natural Gas Leaks and Estimating Their Size: Validation and Uncertainty, *Environ.*  
1036 *Sci. Technol.*, acs.est.8b03135, doi:10.1021/acs.est.8b03135, 2018.

1037 Weller, Z. D., Yang, D. K. and von Fischer, J. C.: An open source algorithm to detect natural gas leaks from mobile methane  
1038 survey data, edited by M. Mauder, *PLoS One*, 14(2), e0212287, doi:10.1371/journal.pone.0212287, 2019.

1039 West, J. J., Fiore, A. M., Horowitz, L. W. and Mauzerall, D. L.: Global health benefits of mitigating ozone pollution with  
1040 methane emission controls., *Proc. Natl. Acad. Sci. U. S. A.*, 103(11), 3988–93, doi:10.1073/pnas.0600201103, 2006.

1041 Xu, L. and Jiang, C.: Initial desorption characterization of methane and carbon dioxide in coal and its influence on coal and  
1042 gas outburst risk, *Fuel*, 203, 700–706, doi:10.1016/J.FUEL.2017.05.001, 2017.

1043 Yacovitch, T. I., Herndon, S. C., Roscioli, J. R., Floerchinger, C., McGovern, R. M., Agnese, M., Pétron, G., Kofler, J.,  
1044 Sweeney, C., Karion, A., Conley, S. A., Kort, E. A., Nöhle, L., Fischer, M., Hildebrandt, L., Koeth, J., McManus, J.  
1045 B., Nelson, D. D., Zahniser, M. S. and Kolb, C. E.: Demonstration of an Ethane Spectrometer for Methane Source  
1046 Identification, *Environ. Sci. Technol.*, 48(14), 8028–8034, doi:10.1021/es501475q, 2014.

1047 Yacovitch, T. I., Herndon, S. C., Pétron, G. P., Kofler, J., Lyon, D., Zahniser, M. S. and Kolb, C. E.: Mobile Laboratory  
1048 Observations of Methane Emissions in the Barnett Shale Region, , doi:10.1021/es506352j, 2015.

1049 Yacovitch, T. I., Neining, B., Herndon, S. C., Van der Gon, H. D., Jonkers, S., Hulskotte, J., Roscioli, J. R. and Zavala-  
1050 Araiza, D.: Methane emissions in the Netherlands: The Groningen field, *Elem Sci Anth*, 6(1), 57,  
1051 doi:10.1525/elementa.308, 2018.

1052 Zavala-Araiza, D., Lyon, D. R., Alvarez, R. A., Davis, K. J., Harriss, R., Herndon, S. C., Karion, A., Kort, E. A., Lamb, B. K.,  
1053 Lan, X., Marchese, A. J., Pacala, S. W., Robinson, A. L., Shepson, P. B., Sweeney, C., Talbot, R., Townsend-Small,  
1054 A., Yacovitch, T. I., Zimmerle, D. J. and Hamburg, S. P.: Reconciling divergent estimates of oil and gas methane  
1055 emissions., *Proc. Natl. Acad. Sci. U. S. A.*, 112(51), 15597–602, doi:10.1073/pnas.1522126112, 2015.

1056 Zazzeri, G., Lowry, D., Fisher, R. E., France, J. L., Lanoisellé, M. and Nisbet, E. G.: Plume mapping and isotopic  
1057 characterisation of anthropogenic methane sources, *Atmos. Environ.*, 110, 151–162,  
1058 doi:10.1016/j.atmosenv.2015.03.029, 2015.

1059 Zhao, W., Zhang, T., Wang, Y., Qiao, J. and Wang, Z.: Corrosion Failure Mechanism of Associated Gas Transmission  
1060 Pipeline., *Mater. (Basel, Switzerland)*, 11(10), doi:10.3390/ma11101935, 2018.

1061 Zimmerle, D. J., Williams, L. L., Vaughn, T. L., Quinn, C., Subramanian, R., Duggan, G. P., Willson, B., Opsomer, J. D.,  
1062 Marchese, A. J., Martinez, D. M. and Robinson, A. L.: Methane Emissions from the Natural Gas Transmission and  
1063 Storage System in the United States, *Environ. Sci. Technol.*, 49(15), 9374–9383, doi:10.1021/acs.est.5b01669, 2015.

1064 Zimnoch, M., Necki, J., Chmura, L., Jasek, A., Jelen, D., Galkowski, M., Kuc, T., Gorczyca, Z., Bartyzel, J. and Rozanski, K.:  
1065 Quantification of carbon dioxide and methane emissions in urban areas: source apportionment based on atmospheric  
1066 observations, *Mitig. Adapt. Strateg. Glob. Chang.*, 24(6), 1051–1071, doi:10.1007/s11027-018-9821-0, 2019.

1067  
1068  
1069  
1070  
1071  
1072  
1073  
1074  
1075  
1076  
1077  
1078  
1079  
1080  
1081  
1082  
1083  
1084  
1085  
1086  
1087



1088 **Table 1: Natural gas distribution network CH<sub>4</sub> emission categories**

Class	CH <sub>4</sub> Enhancement (ppm)	Equivalent Emission Rate (L min <sup>-1</sup> )	Equivalent Emission Rate (≈ kg hr <sup>-1</sup> )	LI Location Colour (Figure 1, Figure 2, and Figure S14)
High	>7.6	>40	>1.7	Red
Medium	1.6-7.59	6 - 40	0.3 – 1.7	Orange
Low	0.2-1.59	0.5 - 6	0.0 – 0.3	Yellow

1089  
 1090  
 1091  
 1092  
 1093  
 1094  
 1095  
 1096  
 1097  
 1098  
 1099  
 1100  
 1101  
 1102  
 1103  
 1104  
 1105  
 1106  
 1107  
 1108  
 1109  
 1110  
 1111  
 1112  
 1113  
 1114  
 1115  
 1116  
 1117  
 1118  
 1119  
 1120  
 1121  
 1122  
 1123  
 1124  
 1125  
 1126  
 1127  
 1128  
 1129  
 1130  
 1131  
 1132  
 1133  
 1134  
 1135  
 1136  
 1137  
 1138

1139 Table 2: Measurements and results summaries across the study area, inside the ring in Utrecht and north Elbe in Hamburg

Study Area		Utrecht (inside the Ring)	Hamburg (North Elbe)			
≈ km street driven	Total km driven	1,000 km	1,800 km			
	Driven once	220 km	900 km			
	Driven more than once	780 km	900 km			
≈ km street covered	Total km covered	450 km	1,200 km			
	covered once	230 km	900 km			
	covered more than once	220 km	300 km			
LIs and emissions	Total number	81 LIs	145 LIs			
	LI density	5.6 km covered LI <sup>-1</sup>	8.4 km covered LI <sup>-1</sup>			
	Total emission rate	290 L min <sup>-1</sup>	490 L min <sup>-1</sup>			
	Average emission rate per LI	3.6 L min <sup>-1</sup> LI <sup>-1</sup>	3.4 L min <sup>-1</sup> LI <sup>-1</sup>			
	Total emission rate per year	107 t yr <sup>-1</sup>	180 t yr <sup>-1</sup>			
LIs visited	Once	Number	16 LIs	45 LIs		
		Emissions	26 L min <sup>-1</sup>	68 L min <sup>-1</sup>		
		Average emission rate per LI	1.6 L min <sup>-1</sup> LI <sup>-1</sup>	1.5 L min <sup>-1</sup> LI <sup>-1</sup>		
	More than once	Number	65 LIs	100 LIs		
		Emissions	264 L min <sup>-1</sup>	423 L min <sup>-1</sup>		
		Average emission rate per LI	4.1 L min <sup>-1</sup> LI <sup>-1</sup>	4.2 L min <sup>-1</sup> LI <sup>-1</sup>		
Total LIs categorized based on von Fischer et al. (2017) categories	High (>40 L min <sup>-1</sup> )	Number	1 LI	2 LIs		
		Emissions	102 L min <sup>-1</sup>	145 L min <sup>-1</sup>		
		Average emission rate per LI	101.5 (L min <sup>-1</sup> LI <sup>-1</sup> )	72.4 L min <sup>-1</sup> LI <sup>-1</sup>		
		% of emissions	35 % of total emissions	30 % of total emissions		
	Medium (6-40 L min <sup>-1</sup> )	Number	6 LIs	16 LIs		
		Emissions	84 L min <sup>-1</sup>	176 L min <sup>-1</sup>		
		Average emission rate per LI	14.0 L min <sup>-1</sup> LI <sup>-1</sup>	11 L min <sup>-1</sup> LI <sup>-1</sup>		
		% of emissions	30 % of total emissions	36 % of total emissions		
	Low (0.5-6 L min <sup>-1</sup> )	Number	74 LIs	127 LIs		
		Emissions	105 L min <sup>-1</sup>	169 L min <sup>-1</sup>		
		Average emission rate per LI	1.4 L min <sup>-1</sup> LI <sup>-1</sup>	1.3 L min <sup>-1</sup> LI <sup>-1</sup>		
		% of emissions	36 % of total emissions	35 % of total emissions		
Total LIs categorized based on OSM road classes	Level 1	Number	6 LIs	29 LIs		
		Emissions	5 L min <sup>-1</sup>	68 L min <sup>-1</sup>		
		Average emission rate per LI	0.76 L min <sup>-1</sup> LI <sup>-1</sup>	2.3 L min <sup>-1</sup> LI <sup>-1</sup>		
	Level 2	Number	16 LIs	34 LIs		
		Emissions	145 L min <sup>-1</sup>	99 L min <sup>-1</sup>		
		Average emission rate per LI	9.0 L min <sup>-1</sup> LI <sup>-1</sup>	2.9 L min <sup>-1</sup> LI <sup>-1</sup>		
	Level 3	Number	3 LIs	23 LIs		
		Emissions	10 L min <sup>-1</sup>	43 L min <sup>-1</sup>		
		Average emission rate per LI	3.4 L min <sup>-1</sup> LI <sup>-1</sup>	1.9 L min <sup>-1</sup> LI <sup>-1</sup>		
	Residential	Number	45 LIs	52 LIs		
		Emissions	93 L min <sup>-1</sup>	274 L min <sup>-1</sup>		
		Average emission rate per LI	2.1 L min <sup>-1</sup> LI <sup>-1</sup>	5.3 L min <sup>-1</sup> LI <sup>-1</sup>		
	Unclassified	Number	11 LIs	7 LIs		
		Emissions	38 L min <sup>-1</sup>	6 L min <sup>-1</sup>		
		Average emission rate per LI	3.4 L min <sup>-1</sup> LI <sup>-1</sup>	0.8 L min <sup>-1</sup> LI <sup>-1</sup>		
	Attribution	C <sub>2</sub> :C <sub>1</sub> ratio analysis	Fossil (Inc. combustion)	% of emissions	93 % of total emissions	64 % of total emissions
				% of LIs	69 % of LIs	33 % of LIs
			Microbial	% of emissions	6 % of total emissions	25 % of total emissions
% of LIs				10 % of LIs	20 % of LIs	
Unclassified			% of emissions	1 % of total emissions	11 % of total emissions	
			% of LIs	21 % of LIs	47 % of LIs	
δ <sup>13</sup> C and δD analysis		Fossil	% of emissions	-----	79 % of total emissions	
			% of LIs	-----	38 % of LIs	
		Microbial	% of emissions	-----	20 % of total emissions	
			% of LIs	-----	54 % of LIs	
		Other	% of emissions	-----	1 % of total emissions	
			% of LIs	-----	8 % of LIs (Pyrogenic)	

CH <sub>4</sub> :CO <sub>2</sub> ratio analysis	Combustion	% of emissions	2 %	10 %	
		% of LIs	7 %	17 %	
	Other	% of emissions	98 %	90 %	
		% of LIs	93 %	83 %	
	C <sub>2</sub> :C <sub>1</sub> ratio, CH <sub>4</sub> :CO <sub>2</sub> ratio, and δ <sup>13</sup> C - δD analyses	Fossil	% of emissions	73 %	48 %
			% of LIs	43 %	31 %
		Combustion	% of emissions	2 %	10 %
			% of LIs	7 %	17 %
Microbial		% of emissions	8 %	35 %	
		% of LIs	4 %	33 %	
Unclassified		% of emissions	16 %	7 %	
		% of LIs	46 %	19%	
Average emission rate per km driven			0.29 L min <sup>-1</sup> km <sup>-1</sup>	0.27 L min <sup>-1</sup> km <sup>-1</sup>	
km driven / total LIs			12.5 km LI <sup>-1</sup>	12.36 km LI <sup>-1</sup>	
Emission factors to scale-up emissions per km covered			0.64 L min <sup>-1</sup> km <sup>-1</sup>	0.40 L min <sup>-1</sup> km <sup>-1</sup>	
km covered per LIs	km covered / total LIs		5.6 km LI <sup>-1</sup>	8.4 km LI <sup>-1</sup>	
	km covered / red LIs		454.8 km LI <sup>-1</sup>	611.4 km LI <sup>-1</sup>	
	km covered / orange LIs		75.8 km LI <sup>-1</sup>	76.4 km LI <sup>-1</sup>	
	km covered / yellow LIs		6.1 km LI <sup>-1</sup>	9.6 km LI <sup>-1</sup>	
km road from OSM (≈ km pipeline)			≈ 650 km	≈ 3000 km	
Up-scaled methane emissions to total roads			420 L min <sup>-1</sup> (≈150 t yr <sup>-1</sup> )	1,200 L min <sup>-1</sup> (≈440 t yr <sup>-1</sup> )	
Bootstrap emission rate estimate and error			420 ± 120 L min <sup>-1</sup>	1,200 ± 170 L min <sup>-1</sup>	
Population in study area			≈ 0.28 million	≈ 1.45 million	
Average LIs emissions per capita (kg yr <sup>-1</sup> capita <sup>-1</sup> )			0.54 ± 0.15	0.31 ± 0.04	
Yearly natural gas consumption			≈ 0.16 bcm yr <sup>-1</sup>	≈ 0.75 bcm yr <sup>-1</sup>	
Fossil emission factors	C <sub>2</sub> :C <sub>1</sub> ratio attribution analysis	Average emission rate per km gas pipeline	0.60 ± 0.2 L min <sup>-1</sup> km <sup>-1</sup>	0.26 ± 0.04 L min <sup>-1</sup> km <sup>-1</sup>	
		Average emission rates per capita	0.50 ± 0.14 kg yr <sup>-1</sup> capita <sup>-1</sup>	0.20 ± 0.03 kg yr <sup>-1</sup> capita <sup>-1</sup>	
	δ <sup>13</sup> C and δD attribution analysis	Average emission rates per km gas pipeline	-----	0.32 ± 0.05 L min <sup>-1</sup> km <sup>-1</sup>	
		Average emission rates per capita	-----	0.25 ± 0.04 kg yr <sup>-1</sup> capita <sup>-1</sup>	
	C <sub>2</sub> :C <sub>1</sub> ratio, CH <sub>4</sub> :CO <sub>2</sub> ratio, and δ <sup>13</sup> C - δD analyses	Average emission rates per km gas pipeline	0.47 ± 0.14 L min <sup>-1</sup> km <sup>-1</sup>	0.19 ± 0.03 L min <sup>-1</sup> km <sup>-1</sup>	
		Average emission rates per capita	0.39 ± 0.11 kg yr <sup>-1</sup> capita <sup>-1</sup>	0.15 ± 0.02 kg yr <sup>-1</sup> capita <sup>-1</sup>	
		Average emission rates / yearly consumption	0.10 – 0.12 %	0.04 – 0.07 %	

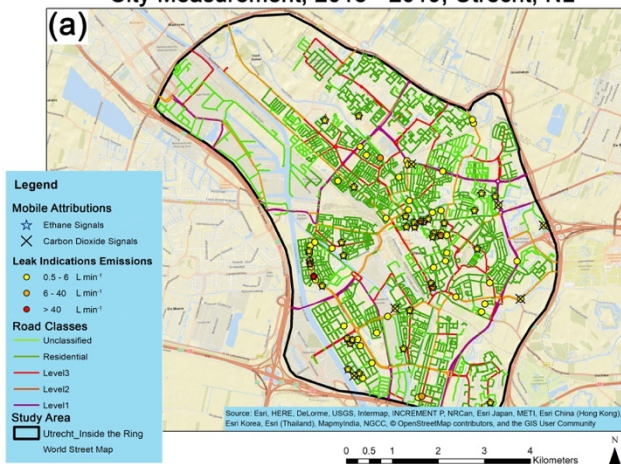
1140  
1141  
1142  
1143  
1144  
1145  
1146  
1147  
1148  
1149  
1150  
1151  
1152  
1153

1154 **Table 3: CH<sub>4</sub> Emissions from larger facilities in Utrecht and Hamburg estimated with the Gaussian Plume model**

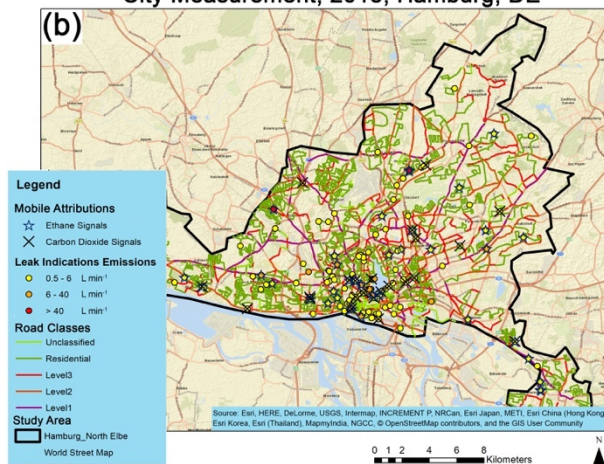
Facility	Emission rate (t yr <sup>-1</sup> )
Utrecht	
Waste Water Treatment Plant (52.109791° N, 5.107605° E)	160 ± 90
Hamburg	
F: Compost and Soil Company (53.680233° N, 10.053751° E)	70 ± 50
Upstream	
D1: 53.468774° N,10.184481° E (separator)	D1: 4.5 ± 3.7
D2: 53.468443° N,10.187408° E (storage tanks)	D2: 5.2 ± 3.0
D3: 53.466694° N,10.180647° E (oil well)	D3: 4.8 ± 4.0

1155  
 1156  
 1157  
 1158  
 1159  
 1160  
 1161  
 1162  
 1163  
 1164  
 1165  
 1166  
 1167  
 1168  
 1169  
 1170  
 1171  
 1172  
 1173  
 1174  
 1175  
 1176  
 1177  
 1178  
 1179  
 1180  
 1181  
 1182  
 1183  
 1184  
 1185  
 1186  
 1187  
 1188  
 1189  
 1190  
 1191  
 1192  
 1193

City Measurement, 2018 - 2019; Utrecht, NL

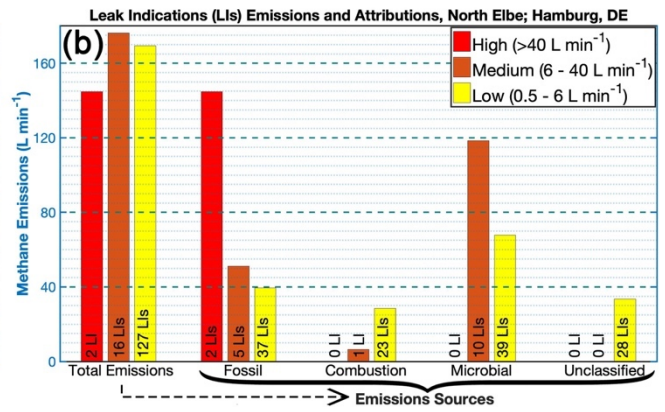
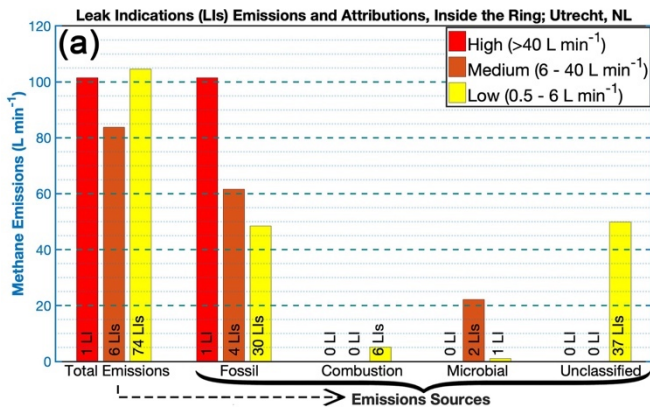


City Measurement, 2018; Hamburg, DE



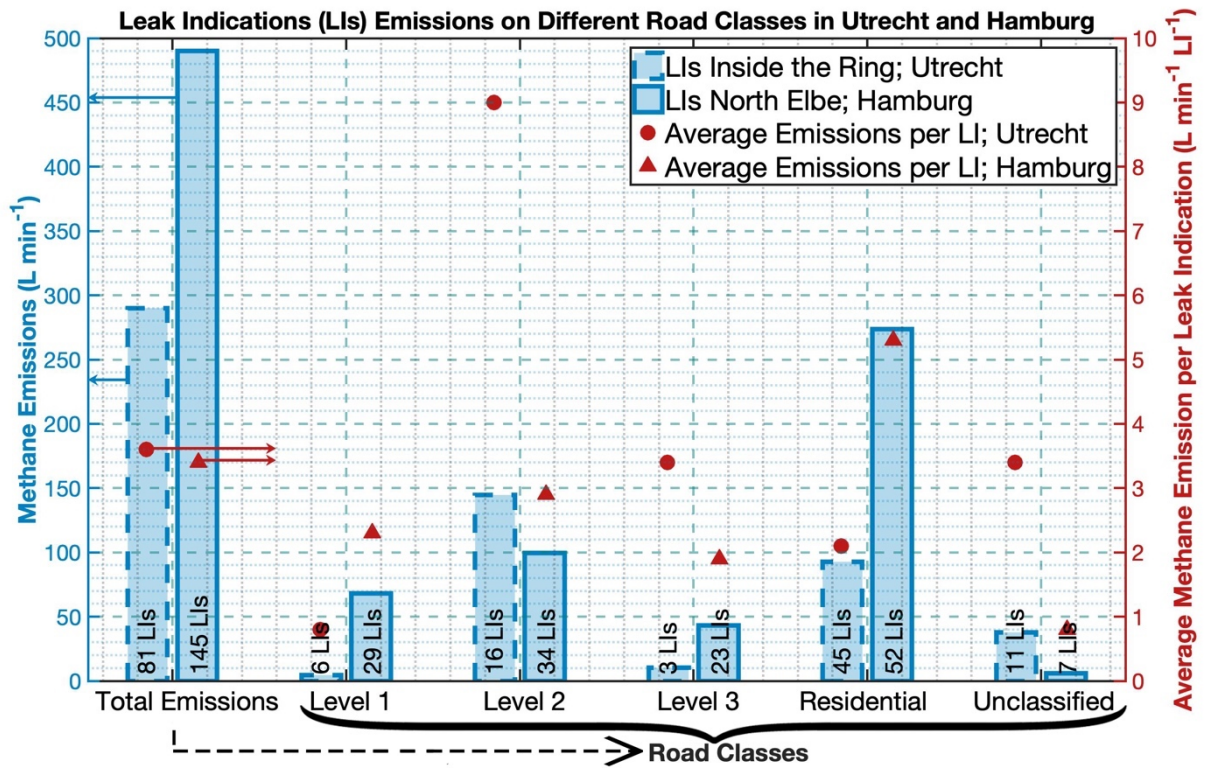
1194  
1195 **Figure 1: Locations of significant LIs for the categories on different street classes in (a) Utrecht and (b) Hamburg. Road colors**  
1196 **indicate the street classes according to the OSM. Black polygons show urban study areas.**

1197  
1198  
1199  
1200  
1201  
1202  
1203  
1204  
1205  
1206  
1207  
1208  
1209  
1210  
1211  
1212  
1213  
1214  
1215  
1216  
1217  
1218  
1219  
1220  
1221  
1222  
1223  
1224  
1225  
1226  
1227  
1228  
1229



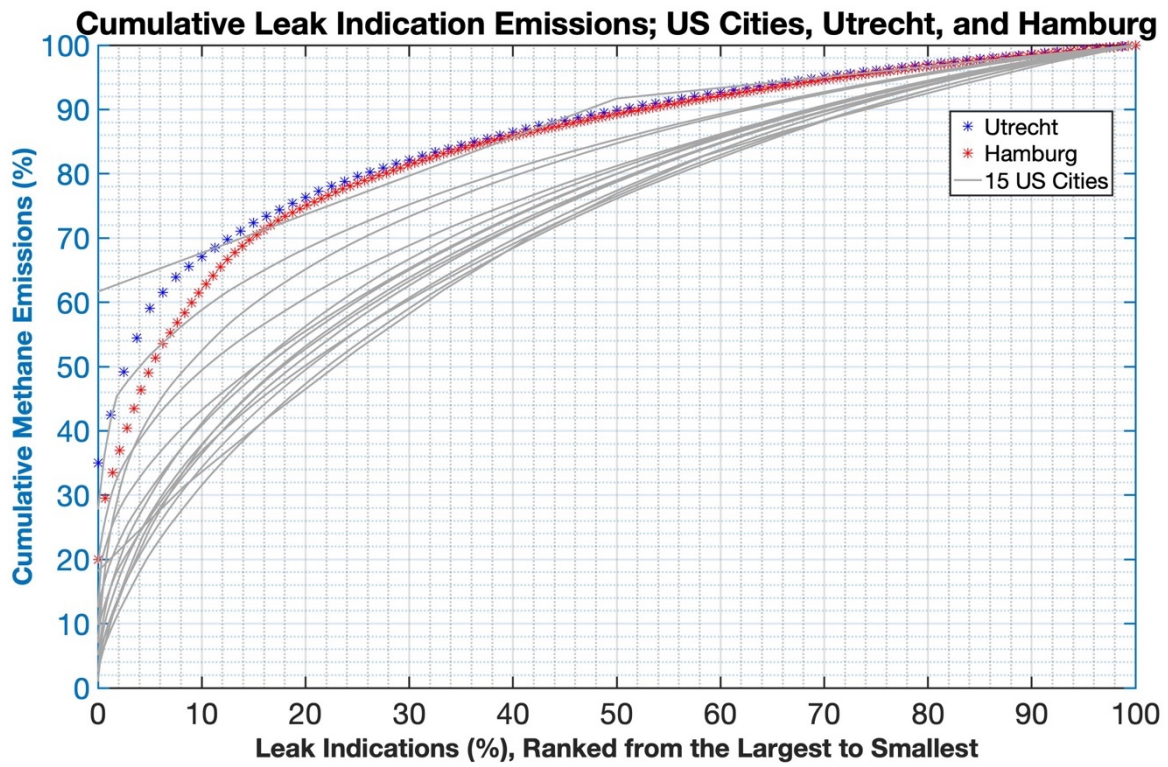
1230  
 1231 **Figure 2: Total CH<sub>4</sub> emission rates from different sources in (a) Utrecht and (b) Hamburg; the arrow shows how the emissions are**  
 1232 **attributed to different sources**

1233  
 1234  
 1235  
 1236  
 1237  
 1238  
 1239  
 1240  
 1241  
 1242  
 1243  
 1244  
 1245  
 1246  
 1247  
 1248  
 1249  
 1250  
 1251  
 1252  
 1253  
 1254  
 1255  
 1256  
 1257  
 1258  
 1259  
 1260  
 1261  
 1262  
 1263  
 1264  
 1265  
 1266  
 1267  
 1268  
 1269  
 1270  
 1271  
 1272  
 1273  
 1274



1275  
 1276 Figure 3: Total CH<sub>4</sub> emissions in Utrecht and Hamburg; the arrow shows how the total emissions are distributed on different road  
 1277 classes

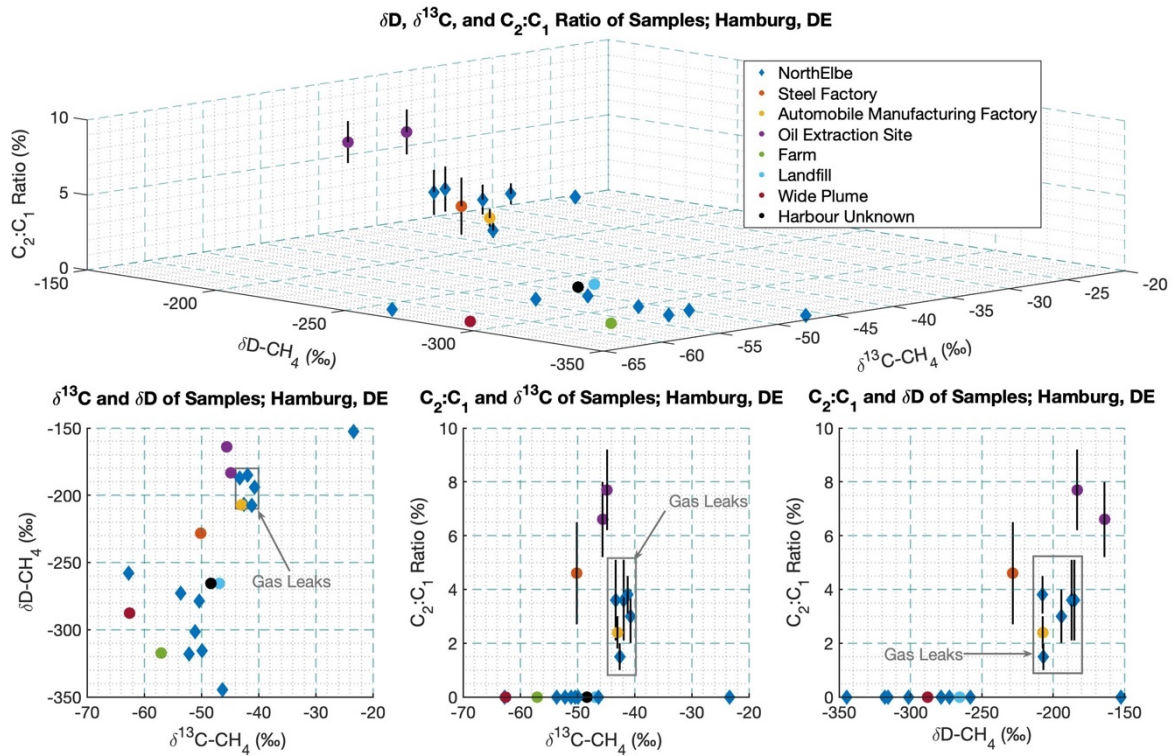
1278  
 1279  
 1280  
 1281  
 1282  
 1283  
 1284  
 1285  
 1286  
 1287  
 1288  
 1289  
 1290  
 1291  
 1292  
 1293  
 1294  
 1295  
 1296  
 1297  
 1298  
 1299  
 1300  
 1301  
 1302  
 1303  
 1304  
 1305  
 1306  
 1307  
 1308



1309  
 1310 Figure 4: Cumulative plot of CH<sub>4</sub> emissions across US cities, Utrecht, and Hamburg; datasets for the US cities are from Weller et  
 1311 al. (2019)

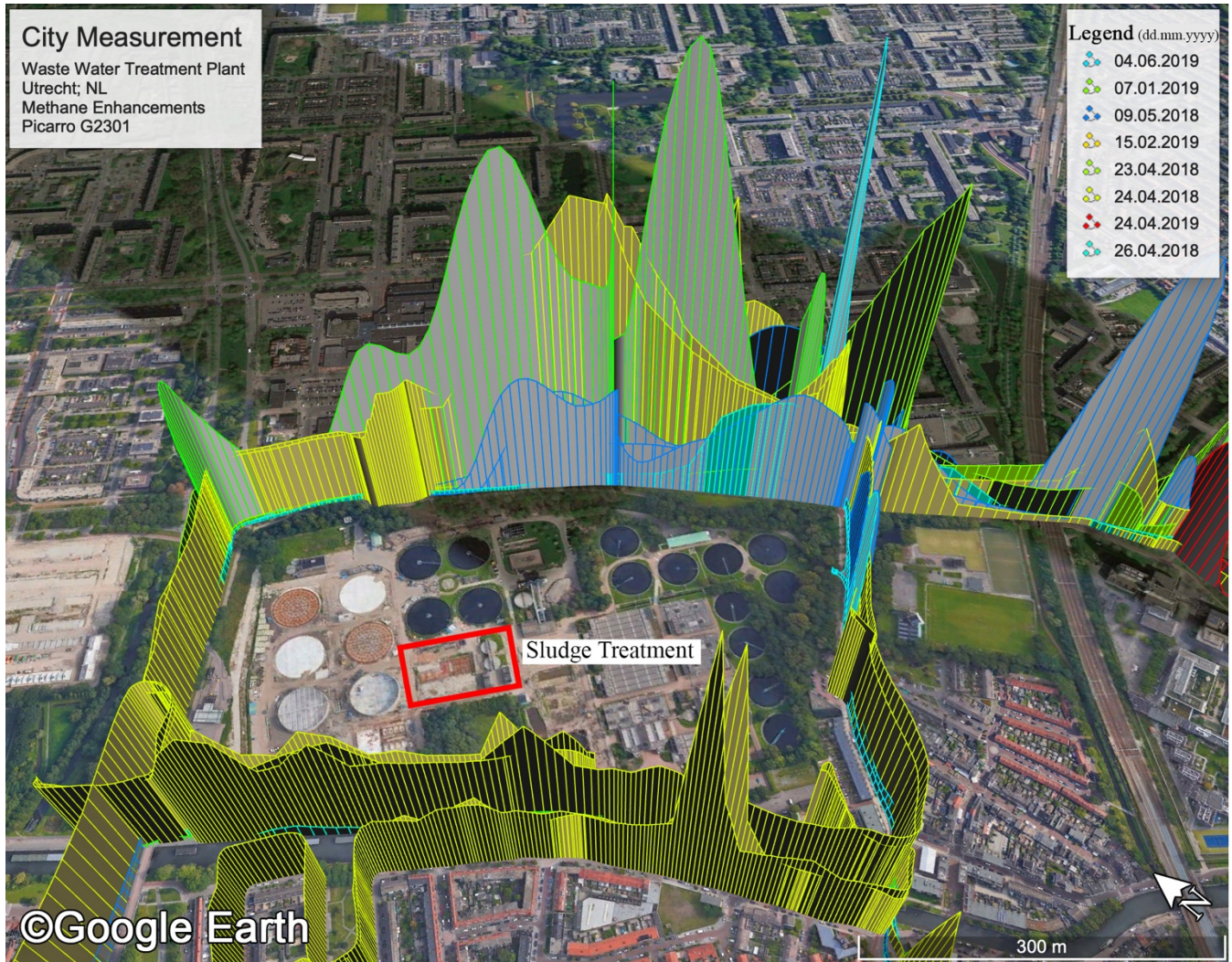
1312  
 1313  
 1314  
 1315  
 1316  
 1317  
 1318  
 1319  
 1320  
 1321  
 1322  
 1323  
 1324  
 1325  
 1326  
 1327  
 1328  
 1329  
 1330  
 1331  
 1332  
 1333  
 1334  
 1335  
 1336  
 1337  
 1338  
 1339





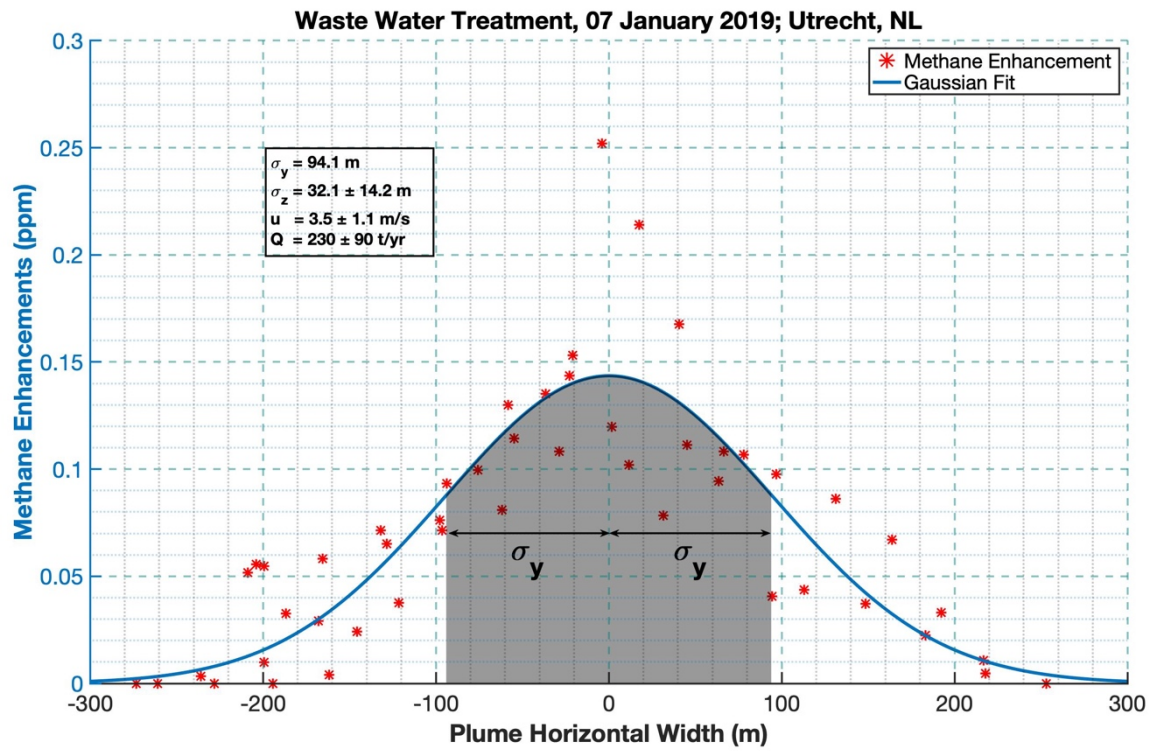
1340  
 1341 **Figure 5: Results from the attribution measurements in Hamburg:  $C_2:C_1$  ratios, and isotopic signatures ( $\delta^{13}C$  and  $\delta D$ ) of collected**  
 1342 **air samples; measurement uncertainties in  $\delta^{13}C$  is 0.05 - 0.1 ‰ and in  $\delta D$  is 2 - 5 ‰**

1343  
 1344  
 1345  
 1346  
 1347  
 1348  
 1349  
 1350  
 1351  
 1352  
 1353  
 1354  
 1355  
 1356  
 1357  
 1358  
 1359  
 1360  
 1361  
 1362  
 1363  
 1364  
 1365  
 1366  
 1367  
 1368  
 1369  
 1370



1371  
 1372 Figure 6: CH<sub>4</sub> enhancements measured downwind waste water treatment plant on Brilledreef street and later used for  
 1373 quantifications from this facility in Utrecht; the centre of the area where the sludge treatment is located was considered as the  
 1374 effective CH<sub>4</sub> emission source, the plumes are plotted on the same scale and max CH<sub>4</sub> enhancement is  $\approx 0.3$  ppm

1375  
 1376  
 1377  
 1378  
 1379  
 1380  
 1381  
 1382  
 1383  
 1384  
 1385  
 1386  
 1387  
 1388  
 1389  
 1390  
 1391  
 1392  
 1393  
 1394



1395  
 1396 Figure 7: Gaussian curve fitted to some transects downwind the waste water treatment plant in Utrecht